CHAPTER 6

NUCLEAR DISINTEGRATION AND RADIATION DETECTION

Radioactive nuclei, produced by neutron activation, disintegrate by beta, gamma, or in some cases alpha, emission. These decay modes may be associated with X-ray and electron emission In this chapter a survey is given of the different modes of decay and the interaction of radiation with matter The usual counting equipment used to measure these radiations is also described.

I. Nuclear Disintegration

(A) Types of Nuclear Decay

1. *Alpha Disintegration*

The alpha particles emitted by radioactive nuclei are physically identical with helium nuclei. Alpha rays are monoenergetic and defined in energy by the two nuclear levels between which they occur. When an excited state of the daughter isotope is obtained by this type of decay, the latter reaches the ground state by gamma emission. Alpha decay mainly occurs in the natural radioactive series, and very seldom when dealing with neutron activated nuclei. The latter happens when a heavy nucleus yields an isotope in the natural series by neutron bombardment, as is the case for the reaction (1)

$$^{209}\mathrm{Bi}(\mathrm{n},\gamma)^{210}\mathrm{Bi} \xrightarrow{\beta^-} {}^{210}\mathrm{Po} \xrightarrow{\alpha}$$

As most alpha rays have energies between 2 and 10 MeV, and the potential barrier of the Coulomb field around the nucleus is much higher, the emission of these particles can be explained only by "tunneling" through the barrier, as is described by Gamow (2). When the potential E as a function of the distance r from the nucleus is represented, as is done in Figure 6.1, wave mechanics permit calculation of the probability of finding a particle with energy E_i at a distance R, outside a nucleus of radius R_A. This probability is given by equation (6.1).

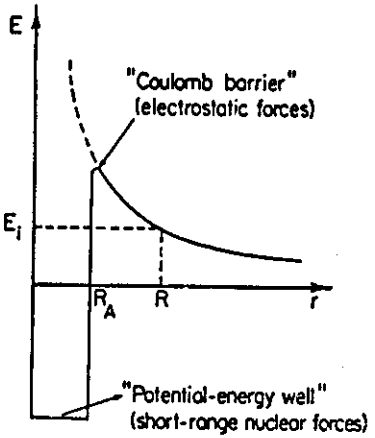

Fig. 6.1. Potential energy E as a function of the distance r from the nucleus. R_A is the nuclear radius.

$$P = \exp\left[-\frac{4\pi}{h}\sqrt{(2m)}\int_{R_A}^{R}\sqrt{(U(r)-E_i)}\,dr\right] \tag{6.1}$$

where h is Planck's constant, m is the reduced mass of the alpha particle and the recoil nucleus and $U(r)$ is the Coulomb barrier as a function of the distance r. From this it is obvious that the probability of emitting an alpha particle increases when the Coulomb barrier decreases or becomes more narrow.

For a decay from even-even nuclei to the ground state or the first excited state of the daughter nucleus, the partial half-life for alpha decay is inversely proportional to the tunneling probability, and to the frequency with which the particle oscillates in the potential well:

$$(t_{1/2})_\alpha \propto \frac{1}{\lambda} \propto \frac{2mR_A^2}{hP} \tag{6.2}$$

All other alpha transitions are normally strongly hindered, the half-life becoming at least a factor of 10^3 larger as indicated by equation (6.2). It is due to this fact that ^{235}U exists in nature and has not completely decayed to ^{231}Th. Alpha transitions of the heavy nuclei in the neighborhood of the magic numbers (e.g. 126) are less strongly hindered, as the nuclear radius increases by about 10% when a nucleon is added to a closed shell. Hence, for these nuclei, which can give rise

by alpha transition to a closed shell daughter isotope the P increases, as the integration limits are closer.

Nuclei decaying by an alpha transition yields daughter isotopes having an atomic number of two units less, whereas the mass decreases by four units. Alpha decay branching occurs when a nucleus decays to several levels of the daughter nucleus.

2. *The Beta Disintegration*

Under the beta disintegration one classifies the types of nuclear decay whereby the active isotope emits a β^- or a β^+ particle. Both particles are physically equal to the electron, differing only through a positive or negative charge. The capture of an orbital electron by the nucleus is also described under this type of disintegration (3,4,5).

(a) The β^- Disintegration. Nuclei emitting β^- particles are often obtained by neutron activation. The stability of the nucleus is in fact related to the proton–neutron ratio. A proton excess causes a Coulomb repulsion, whereas a neutron excess decreases the nuclear forces. Most of the isotopes formed by neutron caption show a neutron excess, which can be annihilated by the reaction

$$n^\circ \rightarrow p^+ + \beta^- + \nu$$

whereby a neutron is transformed into a proton, and a β^- particle together with an antineutrino is emitted. The emitted beta rays are polyenergetic, and show a continuous spectrum starting at energy about zero up to the maximum energy E_{max}. The maximum energy is given by the difference between the two energy levels of the nuclei where the β^- decay occurs. In this case, the antineutrino has zero energy, whereas in all other cases the decay energy is distributed over the β^- particle and the antineutrino.

The beta spectrum for ^{64}Cu is given in Figure 6.2 (6). From Figure 6.2 it appears that the intensity maximum in the spectrum occurs at about $E_{max}/3$.

The β-decay gives rise to a daughter isotope, with an atomic number of one unit less than the parent isotope, whereas the atomic mass stays unchanged. When the daughter nucleus is still in an excited state, it reaches the ground state by emission of one or more gamma rays. These gamma rays are emitted almost immediately after the

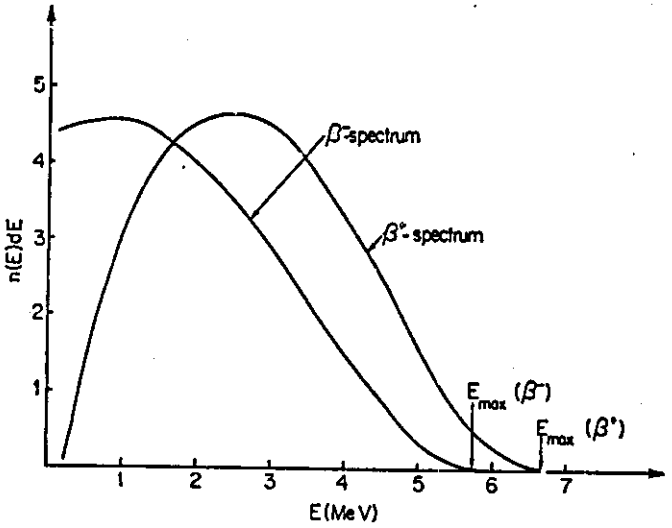

Fig. 6.2. Electron and positron spectrum of the isotope ^{64}Cu (6).

emission of the beta particle, the life times of the excited levels being usually between 10^{-9} and 10^{-13} second.

(b) The β^+ Disintegration. When a nuclear reaction yields an isotope with a proton excess, the probability increases that a proton will be transformed into a neutron according to the reaction

$$p^+ \rightarrow n^\circ + \beta^+ + \nu$$

whereby a positron and a neutrino are emitted. This decay mode occurs mostly with those isotopes of an element, which have a smaller atomic mass than the stable isotope. The energy spectrum of the emitted β^+ particles shows an analogous distribution to that found for the β^- spectra. However, due to the Coulomb repulsion of the nucleus, the lower energies show less intensity and the average energy moves toward the E_{max}, as can be seen in Figure 6.2 where the β^- and the β^+ spectra of the screened nucleus ^{64}Cu are given (6). The neutrino receives also in this type of decay the energy difference between E_{max} and the energy of the emitted β^+ particle.

The β^+ decay gives rise to a daughter nucleus, having a decrease of one unit in atomic number in comparison to the parent isotope, whereas the atomic mass stays unchanged. When the daughter isotope

is still in an excited state, the ground state is reached by emission of one or several gamma rays, similar to the β^- decay.

(c) **Electron Capture.** As the neutron mass is larger than the proton mass ($m_n = 1.008665$; $m_p = 1.007273$), the probability for the transformation of a proton into a neutron, the way it occurs in β^+ decay, increases when the daughter isotope has a lower energy level than the parent isotope. When this energy difference is small, the nucleus can capture an orbital electron, whereby a proton is transformed into a neutron according to the reaction:

$$p^+ + e^- \rightarrow n^0 + \nu$$

The electron, which generally comes from the K-shell (K-capture) neutralizes a positive charge in the nucleus, and the electron rest mass compensates for the mass difference between the proton and the formed neutron. The obtained daughter isotope has an atomic number one unit less than the parent isotope, and can be deexcited by gamma decay. The mass of the daughter nucleus is also in this case practically unchanged.

By the electron capture (E.C.) process one always obtains the characteristic X-ray of the daughter nucleus, due to orbital electron rearrangement. The relation between the energy E of the X-ray in keV and the corresponding wavelength λ in Å is given by $E = 12.395/\lambda$.

A radioactive isotope can decay to several excited states and to the ground state of the daughter nucleus by means of several corresponding β^-, β^+ or E.C. processes. This phenomenon, called branching beta decay, is described in more detail in Section I, B of this chapter.

3. *The Gamma Disintegration*

Gamma rays are electromagnetic radiations, having frequencies which are generally higher than those of X-rays. The nucleus however emits the gamma radiation, whereas the orbital electrons produce X-rays. The relation between the frequency ν and the energy E of a gamma ray is given by $E = h\nu$, where h is Planck's constant.

Gamma rays are monoenergetic, and their energy is completely defined by the energy levels between which they occur. The interaction of gamma rays with matter is however very complicated (3,4,5), so that in general complex spectra are obtained as can be seen from section III, D of this chapter.

(a) **The Gamma Emission.** As described above, gamma emission frequently accompanies beta decay and carries away the energy of the excited levels. The mass and charge of the gamma emitting nucleus are unchanged.

The deexcitation of a daughter nucleus can occur by one gamma ray between the excited and the ground level, or by a cascade of gamma rays between several lower excited levels, or by both. This last phenomenon is also called gamma branching, analogous to the beta branching. As the mean life-time of the excited states is generally short (10^{-9}–10^{-13} s), one can remark that the preceding beta particle and the gammas can be considered as one single cascade. An exception must be made for the first and in some cases the second excited level, which can have a longer life-time and yields an isomeric transition.

(b) **Isomeric Transition–Nuclear Isomerism.** When the gamma transition between the first and in some cases the second excited level and the ground state of a nucleus are highly forbidden, measurable half-lives of these transitions can be obtained. By neutron bombardment not only the ground state but also the first excited state of the nucleus can be formed. Both nuclei are then called mesomeric or isomeric nuclei, whereas the gamma transition between these two states is known as isomeric transition (I.T.). The mesomeric nucleus is indicated with the letter m after the mass number of the isotope (e.g. ^{60}Co, $T_{1/2} = 5.26$y ^{60m}Co, $T_{1/2} = 10$ m and ^{124}Sb, $T_{1/2} = 60$ d; ^{124m_1}Sb, $T_{1/2} = 1.3$ m; ^{124m_2}Sb, $T_{1/2} = 21$ m). When the isomeric state decays to a daughter isotope without going over the ground state, the isomers are called nongenetic. In many cases beta–gamma decay occurs from both the isomeric and ground state of the radioactive nucleus. Sometimes the excited state is even longer lived than the ground state as is the case for ^{110m}Ag, $T_{1/2} = 253$ d whereas ^{110}Ag, $T_{1/2} = 24.4$ s.

(c) **Internal Conversion.** When a gamma ray emerges from the nucleus, interaction with the orbital electrons is possible. An orbital electron of the K, L or M shell is emitted with an energy equal to the gamma energy, minus the binding energy of the electron. These electrons are known as conversion electrons. The orbital electrons are subsequently rearranged, giving rise to an X-ray, which is characteristic for the decaying nucleus. The degree of conversion is dependent upon the atomic number of the nucleus and upon the energy and the type of gamma transition (spin and parity). The percentage converted gamma intensity is given by the conversion coefficients, which are

generally tabulated in the decay schemes (7, 8, 9, 10). Usually the following notations are used:

$\alpha = e/\gamma$ = total fraction of the converted gamma intensity;
$\alpha_{K,L,M} = e_{K,L,M}/\gamma$ = fraction of the gamma intensity converted in K, L or M shell respectively;
$\alpha_{K/L} = e_K/e_L$ = ratio of the number of conversions in the K shell to the number of conversions in the L shell.

The X-rays, which accompany the conversion electrons, can also be converted by the outer electrons. The energies of those conversion electrons (Auger electrons) are only of the order of magnitude of the orbital electron binding energy.

The conversion electrons have the same properties as beta rays, except for the fact that they are monoenergetic.

When using beta counting techniques, conversion electrons can be measured, as can be seen from Figure 6.3, where the conversion electron spectrum of ^{99m}Tc is represented together with the beta spectrum of ^{186}Re and ^{188}Re (11).

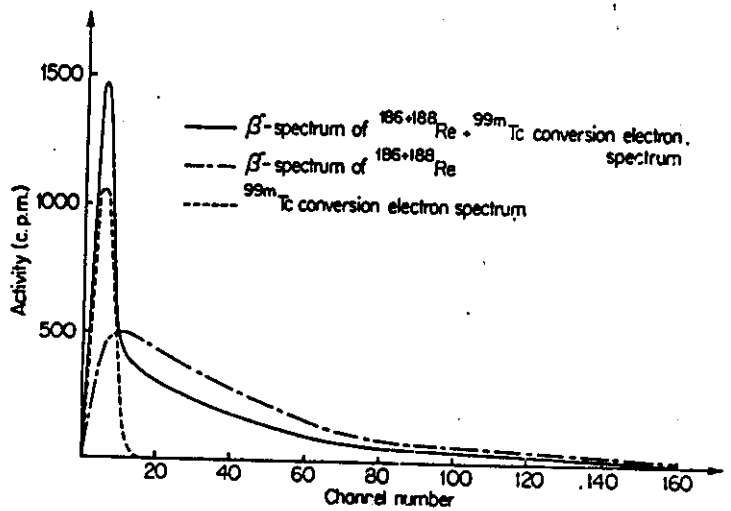

Fig. 6.3. Beta spectrum of $^{186+188}$Re with the conversion electron spectrum of ^{99m}Tc, measured with a 4.4 cm diameter × 0.6 cm thickness plastic scintillation detector (11).

From the several modes of nuclear decay it appears that one can expect three main types of radiation: α rays, β rays and electromagnetic radiation.

(B) The Decay Scheme

The decay mode of a radioactive isotope is represented in a term scheme: the decay scheme, wherefrom a fictive example is given in Figure 6.4.

The energy levels of the different nuclei are drawn as horizontal lines. The relative energies corresponding to the respective ground states are indicated together with the nuclear spin and the parity of the level. The parent and daughter nuclei are represented with increasing atomic number from the left to the right. The atomic number, the mass number, and in the case of an active nucleus also the half-life are indicated next to the symbol of the element.

The β^- decay is represented in this scheme by an oblique line to the right, whereas the β^+ decay is indicated by a broken line to the left and electron capture is given by a straight oblique line also to the left. This shows the implicit change in atomic number with these types of decay. Analogously the alpha decay is indicated by an oblique line going two atomic numbers to the left.

The E_{max} of the β decay and the percentage abundance of a beta ray in the branching is indicated, together with log ft which is a measure of the transition probability (comparative half-life).

The gamma transitions are given by vertical lines, as no change in atomic number occurs. The energy of the gamma ray is obtained by the energy difference of the two levels, between which the transition occurs.

Several types of beta–gamma and gamma–gamma cascades can be seen in the decay scheme ($\beta_1 - \gamma_1 - \gamma_2; \gamma_1 - \gamma_2; \ldots$). These cascades are of particular interest when dealing with coincidence and anti-coincidence countings, as is described in Chapter 6, section III, E. The cascade $\gamma_1 - \gamma_2$ and the simple γ_2 transition are a typical example of gamma branching. Percentage abundances of the different gamma rays are generally listed in a table, added to the decay scheme. These abundances are either given in absolute or in relative values. In the latter case the most abundant gamma is usually taken as unity or 100%.

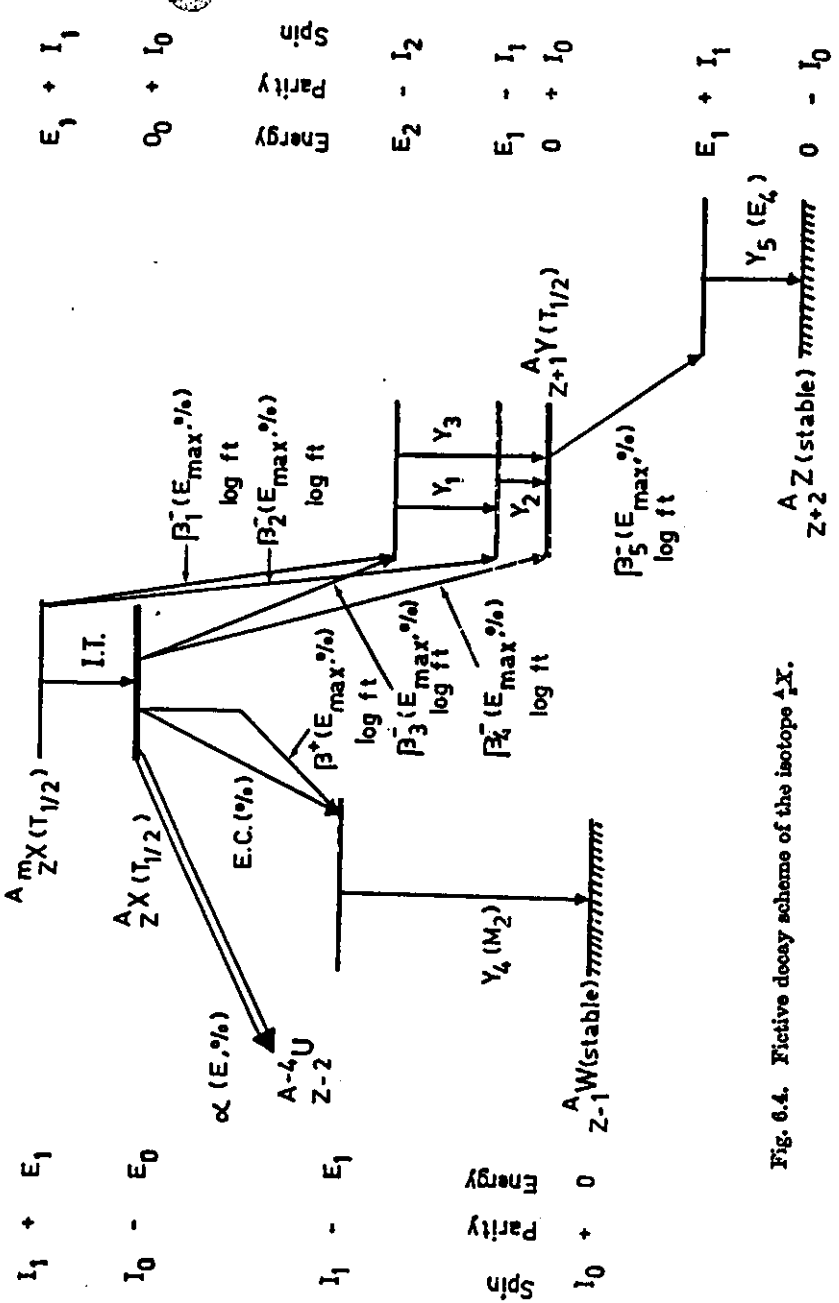

Fig. 6.4. Fictive decay scheme of the isotope ${}^{A}_{Z}X$.

The daughter isotope is not necessarily a stable one, but can also be radioactive, having its own decamode.

Handboks of decay schemes areadily available (7,8,9,10).

C) Selection Rules for Beta and Gamma Transition

When beta or gamma branchi occurs, the probability of the different possible transitions is rulesby their state of "forbiddenness", which can be derived from the seleon rules. The allowed transitions are divided into favored or unfaved, whereas the forbidden transitions are subdivided into a degree of forbiddenness (first order, second order . . .), the transition probility decreasing with increasing order. An increaseof one unit in tlorder of forbiddenness generally increasesthe halflife of the transin by a factor of 100.

The two factorsdominating the ection rules are the nuclear spin and the parity of the energy levels. The nuclear spin I is the vectorial sum of the orbita and the spin aular momentum of all nucleons present in the nucleus. Isotopes with even atomic numbers have integral spin numbers, whereas odd atomic numbers give rise to half integral spin numbers. Analogously the fundamental particles, the different energy levels of the nucleus have the property of a positive or negative parity, indicated respectively with a + or − sign next to the spin number. Positive parity occurs, when the spatial coordinates of the wave function, which expresses the probability of finding a nucleus in a givenenergy state, indicated by its coordinates, can be multiplied by −1 without change in sign of the function. In the opposite case negative parity occurs. When a transition the lower level has an opposite paritysign from the upper level, one indicates a "yes" parity change. A parity change "no" is noted when both levels show the same parity sign.

1. *Selection Rules for Beta Transition*

The selection rules for the beta transition have been described by Fermi (12 and also by Gamow andTeller (13). The total probability for a beta transition between two energy levels is given by the integral between $I = 0$ and $E = E_{max}$ of the differential probability of an electron having an energy between E and $E + dE$.

As f is rather a complicated function, empirical formulas have been derived for the different types of beta decay:

$$\log f_{\beta^-} = 4.0 \log E_{max} + 0.80 + 0.08\,Z - 0.005\,Z \log E_{max} \quad (6.3)$$

$$\log f_{\beta^+} = 4.0 \log E_{max} + 0.80 - 0.007\,Z - 0.009\,Z\left(\log \frac{E_{max}}{3}\right) \quad (6.4)$$

$$\log f_{E.C.} = 2 \log E_{max} + 3.5 \log Z - 5.6 \quad (6.5)$$

These formulas are valid for atomic numbers Z between 0 and 100, and for E_{max} between 0.1 and 10 MeV.

As the f function expresses the total probability of a transition between two energy levels, it has to be proportional to the partial half-life t of the upper level:

$$\frac{\ln 2}{t} = \lambda = Kf \quad (6.6)$$

where K is constant for a given type of transition and λ is the partial decay constant of the given level. One can remark that Sargent's rule (14)

$$\lambda = kE_{max}^5 \quad (6.7)$$

is a special case of equation (6.6).

From relation (6.6) it appears that ft is a constant for a given transition, and will determine which type of transition is dealt with. In the decay schemes one generally indicates log (ft), which has a value 3 to 6 for allowed transitions and 6 to 10 for forbidden ones of the first order (15).

The combination of the change in spin and parity and the log ft value constitute the criterion for the degree of allowance or forbiddenness of a given transition. A schematic table of several types of transitions as a function of these three parameters is given in Table 6.1.

2. *Selection Rules for the Gamma Transition*

Theory and experiment agree that the gamma transition life-time, which is a measure of the probability of the decay, depends upon the gamma energy, the change in nuclear spin and parity, the degree of internal conversion and the atomic mass. The transition can be classified as electric or magnetic, which is represented respectively by E_n or

M_n, n indicating the polarity or the multipolar order ($n = 1$ is a dipole; $n = 2$ is a quadrupole; . . .). In the decay schemes the kind and the polarity of the gamma transition are often indicated next to the gamma ray. The E_2 type is the most frequently occurring.

In view of the large number of variables it is easily understood that the calculation of the gamma transition probabilities is tedious and approximate. Practically, the calculation as well as the experiments lead to the following conclusions:

The probability of gamma emission is directly proportional to the energy difference between the two levels, and inversely proportional to the multipolar order.

The probability of internal conversion decreases with increasing energy and increases with multipolar order and atomic number.

From this it appears that the partial half-life for a given gamma transition is directly proportional to the gamma energy, and inversely proportional to the change in nuclear spin, which is related to the multipolar order. At low energies and high multipolar order, the transition becomes highly forbidden and measurable half-lives exist, which give rise to nuclear isomers, and isomeric transition.

TABLE 6.1

Classification of the beta transition selection rules according to Konopinski (16)

Transition	Parity change	Change in nuclear spin I: Gamow–Teller	Change in nuclear spin I: Fermi	Approximate log ft
Allowed	no	0, ± 1 (except 0 → 0)	0	3–6
First-forbidden	yes	0, ± 1, ± 2 (except 0 → 0, 1/2 → 1/2 0 ↔ 1)	(except 0 → 0)	6–10
Second-forbidden	no	± 2, ± 3, 0 → 0 (except 0 ↔ 2)	± 1, ± 2 (except 0 ↔ 1)	>10
nth-forbidden		± n, ± (n + 1)	± (n − 1), ± n	
n odd	yes			
n even	no			

II. Interaction of Radiation with Matter

The interaction of radiation with matter is dependent on the type and energy of the radiation, and on the physical properties of the interacting material. The transmitted activity A of a radioactive point source with activity A^0, after passing through t cm of material is approximately given by the classical exponential law:

$$A = A^0 \exp(-\mu' t) \tag{6.8}$$

The linear attenuation coefficient μ' (in cm^{-1}) is a function of the interacting material, and the type and energy of the radiation.

For practical purposes, the mass attenuation coefficient $\mu = \mu'/\delta$ (in $cm^2\ mg^{-1}$) is used, where δ is the density of the medium. This includes that the attenuation thickness d must be expressed in mg cm^{-2}, whereby μ becomes independent of the density and the physical state of the medium, and equation (6.8) becomes

$$A = A^0 \exp(-\mu d) \tag{6.9}$$

The processes whereby the radiation energy is transferred to the medium are, however, completely different for alpha particles, electrons, positrons and electromagnetic radiation.

(A) Interaction of Alpha Particles

When passing through matter, alpha particles loose their energy mainly by excitation and ionization of atoms and molecules. The electrons produced in the latter process, the so called delta rays, are energetic enough to give rise to secondary ionization, the average energy of an electron, produced by an ionizing alpha collision being of the order of 100 eV. Due to their heavy mass and large electrical charge, alpha particles have relatively short ranges. On the other hand, as these particles loose only a small fraction of their energy in a single collision, they are not appreciably scattered and their paths are straight tracks. Furthermore, alpha particles are high energetic and a very large number of collisions is required to bring them to rest (about 10^5 for a particle of a few MeV), resulting in the fact that all particles of a transition give the same range within narrow limits. This absorption process, which is similar for all charged particles, heavier than the electron, explains why the alpha absorption does not follow the general equation (6.9).

The small fluctuations (generally 3–4%), which are obtained from the main range are caused by the so-called straggling of the alpha particles (17). This is due to the statistical fluctuations in the number of collisions, and the energy loss per collision as well as to the varying state of ionization of the alpha particle. Ranges of alpha particles are normally determined by measuring the distance they travel in air, or by absorption in a gas at different pressures, which is more accurate.

The relationship between the range R_a of an α-particle in air at N.T.P., and its initial velocity v_0 is given by Geiger's formula:

$$v_0^3 = aR_a \tag{6.10}$$

where R_a is expressed in cm, v_0 in cm s^{-1} and a is an empirical constant equal to 1.08×10^{27}. Hence the energy of the particle as a function of R_a is given by

$$E^2 = 10.68\ R_a^2 \tag{6.11}$$

(B) Interaction of Electrons and Positrons

The corpuscular character of electrons and positrons and their electrical charge is responsible for their high ionizing and hence for their small penetrating power or range in an absorbing material. Electrons of 1 MeV energy are completely stopped in 1.5 mm of aluminium. Beta rays lose their energy by radiation as well as by inelastic scattering.

When beta rays interact with the field of a nucleus, they lose energy by emission of X-rays, so called "Bremsstrahlung". This radiation shows a continuous spectrum, extending from zero to the maximum energy of the interacting beta ray.

The conversion of kinetic energy into Bremsstrahlung is proportional with the energy of the beta particle and with the square of the atomic number of the interacting nucleus. In most cases this phenomenon is produced in the source material itself, so that with the beta rays Bremsstrahlung X-rays are also emitted. Bremsstrahlung is produced by beta rays having an energy of 100 keV and larger. At lower energies elastic and inelastic scatter mainly occur. By inelastic collisions kinetic energy of the electron is transferred, with or without primary ionization of the medium, giving rise to secondary electrons or delta rays.

The total mass absorption coefficient will be composed of the sum of the probabilities of the different effects. As a beta spectrum is

continuous the exact evaluation of the total absorption coefficient is generally experimentally determined. Gleason *et al* (18) give an empirical relation between the mass absorption coefficient μ and the E_{max} of the beta emission, expressed in MeV:

$$\mu = 0.017\, E_{max}^{-1.43} \qquad (6.12)$$

The relation is claimed to be valid for 0.1 MeV $< E_{max} <$ 2.5. MeV. Combination of (6.9) with (6.12) permits in a simple way the evaluation of the beta ray absorption.

When a positron interacts with matter, it loses its kinetic energy very rapidly by one of the described processes, and eventually reacts with a free electron in such a way that the rest mass of both particles is converted into gamma radiation. This effect is called the annihilation of the positron, and the gamma rays are called annihilation radiation. According to the conservation of mass and momentum, each annihilation yields two gamma rays of 0.511 MeV, which are emitted at an angle of 180°. Due to the small penetrating power of the positron, annihilation also occurs in the source material. From this it is clear that the annihilation gamma rays are always detected, when dealing

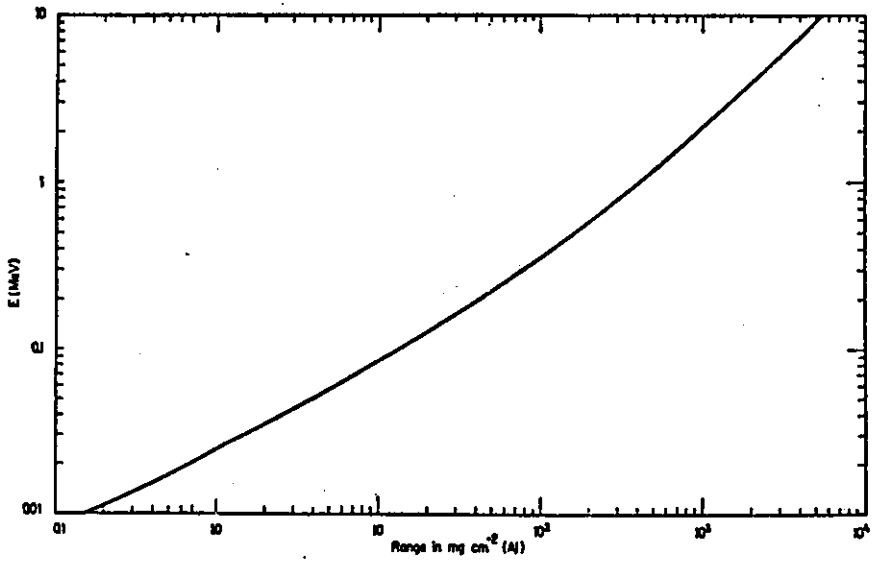

Fig. 6.5. The range of beta rays in aluminium as a function of beta energy.

with a positron emitter, even when the daughter isotope emits no gammas at all.

It is obvious that by the absorption of energetic positrons or electrons, X-rays or gamma rays are always produced, which are not completely stopped in the absorbing material. The distance that electrons as well as positrons travel in aluminium, the so called range, is represented in Figure 6.5. As the range is expressed in mg/cm², these data also apply approximately to other absorbing materials.

(C) Interaction of Electromagnetic Radiation

Due to the wave character, the electromagnetic radiation penetrates more deeply in matter than electrons or positrons. Gamma and X-rays have an ionizing power of about two orders of magnitude less than beta rays of the same energy. The electromagnetic radiation reacts with matter according to the following processes: photoelectric effect, Compton effect and pair production.

1. *Photoelectric Effect*

Low energy photons and X-rays lose their energy by one photoelectric interaction, whereby the total energy of the radiation is transferred to the photoelectron. About 80% of the interactions occur with K-electrons and the other 20% with L-electrons. Photoelectric interaction with "free electrons" is impossible as the recoil of the atom must exist for the conservation of energy and momentum. The electron energy is equal to the absorbed photon energy minus the binding energy of the electron. Almost immediately the orbital electrons are rearranged and an X-ray is emitted, characteristic for the absorbing material, with an energy equal to the binding energy of the photoelectron.

The probability of photoelectric interaction is approximately proportional to Z^4 of the absorber and to E^{-3} of the interacting photon. Thus, the photoelectric effect mainly occurs with high Z absorbers and low photon energies.

2. *Compton Effect*

The Compton effect is the reaction whereby a photon collides with a "free electron", which is an electron from the outer orbital of the

interacting atom. During this collision, part of the gamma energy is transferred to the electron, whereas the gamma ray, which is now less energetic, is deflected through an angle θ with respect to the incident direction. The energy of the gamma ray after collision, E_γ, is a function of the scatter angle θ, and is given by

$$E_\gamma = \frac{E_0}{1 + (E_0/m_0c^2)(1 - \cos\theta)} \tag{6.13}$$

where E_0 indicates the incident gamma energy and m_0c^2 the rest mass of the electron. The deflected gamma can undergo other Compton processes and/or a photoelectric interaction.

The energy of the Compton electron E_e is then found by:

$$E_e = E_0 - E_\gamma \tag{6.14}$$

As E_γ can vary continuously between a minimum for $\theta = 180°$ and a maximum for $\theta = 0°$, the Compton electron energy spectrum extends from zero energy up to a maximum energy given by

$$E_{e_{max}} = \frac{E_0}{1 + \dfrac{m_0c^2}{2E_0}} \tag{6.15}$$

In Compton interactions, absorption as well as scatter phenomena occur. At a gamma energy of about 1.6 MeV both phenomena have equal probability. At higher energies absorption dominates, whereas the inverse occurs at lower energies.

The probability of Compton interaction increases with increasing Z of the absorber and with decreasing energy of the gamma radiation.

3. *Pair Production*

A gamma ray having an energy larger than 1.02 MeV can interact with the Coulomb field of an absorber nucleus and give rise to an electron–positron pair. The total energy of the absorbed gamma ray, minus the rest mass of the particles ($2\ m_0c^2 = 1.02$ MeV) is divided between the pair.

When the positron has lost its kinetic energy, it annihilates under emission of two 0.511 MeV gamma rays. These gammas in turn can give rise to photoelectric absorption or Compton interaction. The probability of pair production with gamma rays is, up to about 5 MeV, directly proportional to Z^2 of the absorber atoms and is a function of the gamma energy.

4. *Attenuation Coefficients*

The total linear attenuation coefficient μ' (in cm^{-1}) for electromagnetic radiation is composed of three attenuation coefficients:

$$\mu' = \tau + \sigma + \kappa \tag{6.16}$$

where τ = attenuation coefficient for photoelectric interaction;
σ = attenuation coefficient for total Compton interaction;
κ = attenuation coefficient for pair production.

Figure 6.6 represents the linear attenuation coefficients for NaI, Ge and Pb as a function of gamma ray energy.

The total linear attenuation coefficient is a measure of the number of primary photons which have interactions. It should not be confused with the total *absorption* coefficient, which is always smaller and is a measure of the energy absorbed by the medium.

A summary of the possible combinations, occurring in the decay of an active isotope, and the interaction of the emitted radiation with matter, is given by Schulze (19) and represented in Table 6.2.

III. Radiation Detection

(A) Types of Detectors

1. *Gas Filled Detectors*

Under gas filled detectors one classifies those counters which make use of gas amplification produced by secondary ionization. Depending upon the construction and upon the electric field, the secondary ionization can be proportional or not to the primary one. In the first case a proportional counter and in the other case a Geiger–Müller counter is obtained.

(a). The Geiger–Müller Detector. The G–M detector is still widely used as a beta counter. Usually, this detector consists of an earthed metallic or graphite cylinder with an insulated central anode wire. The counter is filled with a gas, which interacts with the penetrating

can be made to match the emitted luminescence with the spectral properties of the P.M. The decay time in this type of scintillator is however much larger than in organic crystals as can be seen from Table 6.4.

3. *Semiconductor Detectors*

The semiconductor detectors contain a group of detectors in which the charges, produced by absorption of the incident radiation in a semiconductor material, are collected (28,29). They can be compared to a gas ionization chamber. When atoms are arranged close together in a crystal lattice, the energy levels of the electrons in the atom split up, due to the Pauli principle, and give rise to energy bands, as is schematically shown in Figure 6.11.

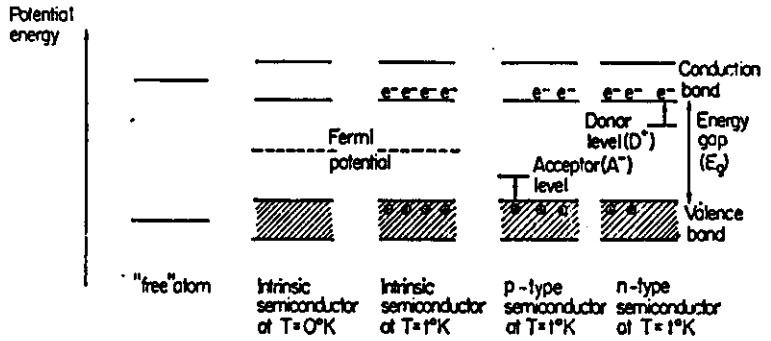

Fig. 6.11. Electron energy levels in a semiconductor.

At absolute zero temperature the electrons in insulators and semiconductors fill up completely one or more of the lowest energy levels, the highest filled level being called the valence band. This band is separated from the next higher one, the conduction band, by a gap of forbidden energies E_g, so that no conduction can occur. At any higher temperature there will be some thermal excitation of electrons from the valence band into the conduction band, leaving empty places or "holes", carrying a positive charge. With electrons falling back to the valence band a dynamic equilibrium is reached, which is a function of temperature. The occupation probability of a level at energy E is given by the Fermi function:

$$f(E) = \frac{1}{1 + \exp\left[(E - \zeta)/kT\right]} \tag{6.25}$$

where k is Boltzmann's constant, T the absolute temperature and ζ the Fermi potential, i.e. the potential where the occupation probability of an allowed state would be 0.5. In an intrinsic or pure semiconductor, the Fermi level must be in the center of the forbidden energy gap. When an electric field is applied holes and electrons move to their respective electrodes, resulting in conductivity. The absorption of radiation energy creates such electron-hole pairs and the collection of these charge carriers gives rise to an output signal, proportional to the amount of energy absorbed. To obtain the equivalent of one electron charge to the output pulse 40 eV are needed in gas detection, 300 eV in NaI(Tl) and up to 5 keV in organic scintillation detectors. In semiconductor detectors however only a few electronvolts are needed (3.6 eV in Si and 2.9 eV in Ge) for impact ionization, including the small energy losses due to the formation of Raman phonons in the crystal lattice. The fact that only a few electronvolts are needed in order to obtain the equivalent of one electron charge, implies that the statistical distribution of the transformation of radiation energy into electrical energy considerably improves, which explains the excellent resolution of the semiconductor detectors.

Semiconductor material contains some impurities, which can be of the donor or the acceptor type, resulting in intermediate levels in the forbidden energy region, as can be seen in Figure 6.11. A donor impurity has the tendency to give electrons to the conduction band, whereas an acceptor takes electrons out of the valence band, resulting in hole creation. A donor or n-type will thus have an excess of electrons, whereas an acceptor or p-type will show an excess of positive holes. Donor and acceptor atoms form together with other impurities and lattice imperfections "trapping centers" where charge carriers can be trapped for times longer than the dielectric relaxation time or can give rise to recombination with carriers of the opposite sign. Trapping and recombination both affect the proportionality between absorbed energy and output pulse amplitude. Dearnaley and Northrop (28) summarize the properties required to obtain a good counter as follows:

Low carrier density to minimize noise. The carrier density being a function of the counter volume, the energy gap and the temperature, a gap of 1.4 eV for a 1 cm³ detector at room temperature is required.

Absence of "trapping center" to minimize loss of signal.
High carrier mobilities and long carrier life-times to obtain short pulse rise-times and efficient charge collection.
Low energy per produced ion pair, to optimize the resolution.
High atomic number for high stopping power of the radiation.

It is obvious that some of these properties are in conflict with each other, and one will have to compromise in order to obtain the optimum working conditions. According to the same authors, a survey of the properties of some semiconductor materials is given in Table 6.5.

Thus far, only homogeneous or bulk detectors were considered. The major difficulty in obtaining such a counter is to have material with sufficiently low carrier density. Therefore n or p type semiconductor material can be compensated with acceptor or donor atoms in order to simulate an intrinsic material (30). This, of course, introduces trapping centers into the material, resulting in a proportionality loss.

Different solutions were applied to obviate these difficulties, namely diffused junction, surface barrier and p.i.n. detectors, as shown in Figure 6.12. The diffused junction detector consists of p and n type

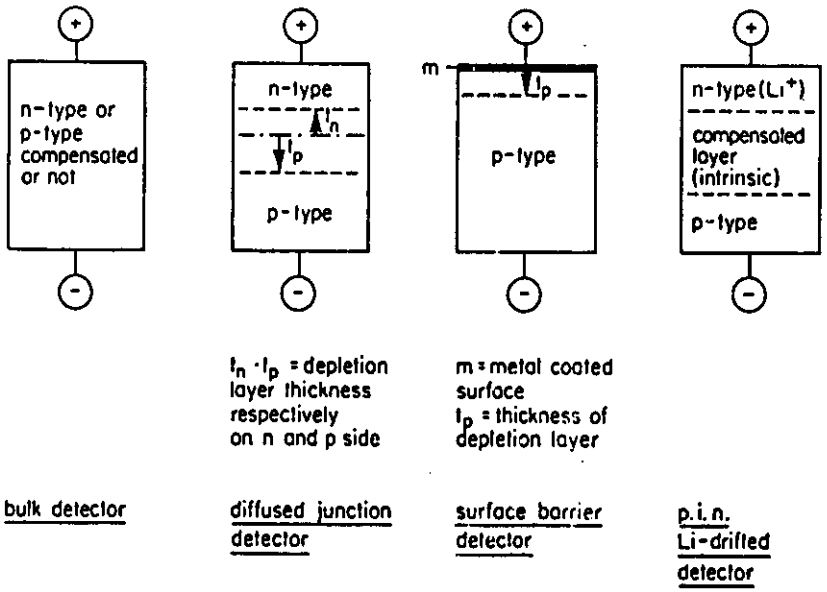

Fig. 6.12. Different types of semiconductor detectors.

TABLE 6.5
Properties of some semiconductor materials (28)

Semiconductor	Energy gap at 300°K (eV)	Electron mobility at 300°K ($cm^2\ volt^{-1}\ s^{-1}$)	Hole mobility at 300°K ($cm^2\ volt^{-1}\ s^{-1}$)	Electron life-time in p-type (s)	Hole life-time in n-type (s)
Silicon	1.08	1500	500	3×10^{-3}	3×10^{-3}
Germanium	0.67	3800	1800	10^{-3}	10^{-3}
Gallium arsenide	1.43	8500	420	10^{-7}	10^{-7}
Gallium phosphide	2.25	140	150	10^{-3}	10^{-3}
Cadmium telluride	1.5	$\simeq 100$	$\simeq 100$	4×10^{-5}	$> 10^{-5}$
Indium antimonide	0.17	78,000	750	$\simeq 10^{-7}$	$\simeq 10^{-7}$
Gallium antimonide	0.67	4000	1400	$\simeq 10^{-5}$	$\simeq 10^{-5}$

material, obtaining in this way a rectifying junction. The detector is used in the reverse direction, this means with the n side biased positive, helping in this way the built in field to remove free charges from the junction interface and from the regions on either side of it. This effect creates a so called "depletion layer" which constitutes the active volume of the counter. In this layer the free carrier concentrations are below their thermal equilibrium numbers, thus reducing the residual current. It should be noted that the depletion layer thickness t, on the n and the p sides, is a function of the resistivity ρ of the counter and the applied bias voltage V:

$$t = \left(\frac{\kappa\mu}{2\pi}\rho V\right)^{1/2} \text{ cm} \qquad (6.26)$$

where κ is the dielectric constant of the material and $\mu = \mu_n$, the mobility of the electrons in n-type material, or μ_p, the hole mobility, when dealing with a p-type material. It is obvious that the detector has to operate with a stable bias voltage.

In surface barrier detectors, the so called Schottky barrier is obtained by coating the surface of semiconductor material with a thin metal layer (31,32). This process, performed at ambient temperature, yields detectors with a better resolution than the diffused junction detector, where the diffusion is carried out at higher temperatures (800–1000°C for Si). The surface barrier detectors, although in other properties analogous to the diffused junction detectors, have the advantage that the depletion layer is on the surface, avoiding energy loss of the incident radiation through the bulk of the material.

Another type of detector which has proved to be extremely useful in gamma ray spectroscopy is the p.i.n. junction. In this type a compensated layer is produced between the n and the p side of the detector, giving rise to an "intrinsic" layer of considerable thickness. Widely used are p-type Si or Ge, in which Li has been diffused and drifted by means of an external field at a temperature where the diffusion is still low (33,34). In this way an "intrinsic" layer is obtained between the p-type material and the n-type diffused region. In this layer the concentration of negative acceptor ions is compensated by the positive lithium donor ions. It should be noted that all germanium counters require cooling with liquid nitrogen. Although silicon counters can be operated at room temperature, better resolutions are obtained at

dry ice temperature. A summary of some applications and properties of the semiconductor detectors is given in Table 6.6.

As the output pulses of the detector are of the order of millivolts, preamplification becomes necessary. Figure 6.13 shows two types of

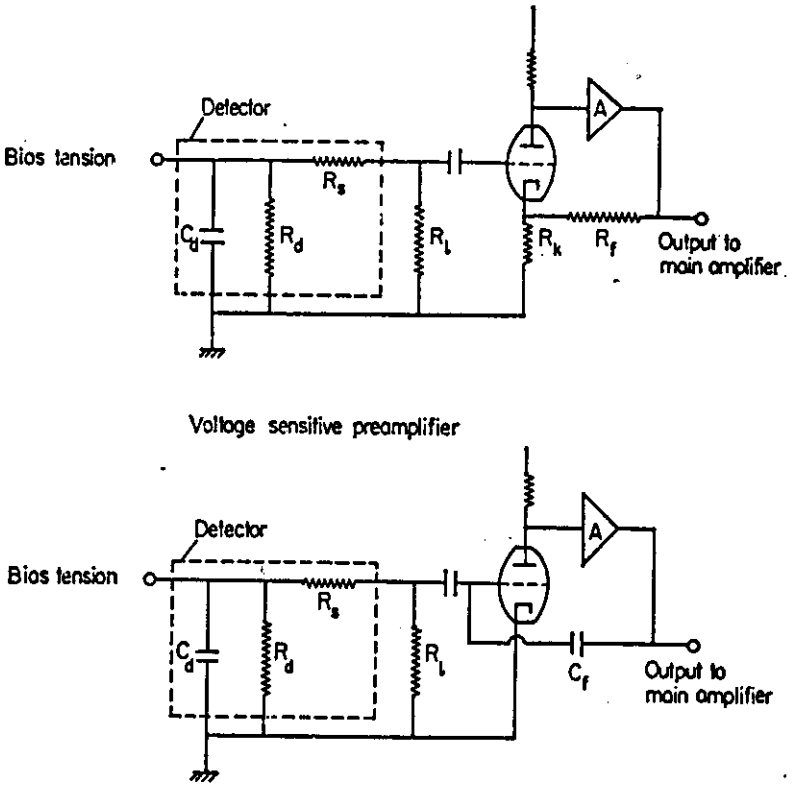

C_d R_d and R_s Capacitance parallel and series resistance of the detector
R_l Load resistor
R_K Cathode resistor
R_f and C_f Feedback resistor and capacitor
A Preamplifier

Fig. 6.13. Principle of a voltage and a charge sensitive preamplifier for use with semiconductor detectors.

TABLE 6.6
Some properties and applications of semiconductor detectors (28)

Type of junction	Semiconductor material	Sensitive thickness or volume	Typical resolution (KeV FWHM)	Applications
Diffused junction	Si high resistivity long life time	up to 1 mm	20 keV for 5 MeV alphas	monitoring, health physics (low resolution applications)
Surface barriers	Si high resistivity long life time	up to 2 mm	3.8 keV for ^{137}Cs betas 11 keV for 6 MeV alphas	high resolution charged particle spectrometry (beta and alpha spectrometry)
Lithium drifted p-i-n. junction	Ge or Si high sensitivity long life time	up to 50 cm^3	*silicon:* 3.8 keV for ^{137}Cs conv. el. (624.15 keV) 300 eV for ^{241}Am gamma (59.57 keV) 15 keV for 6 MeV alphas *germanium:* 3.5 keV for ^{137}Cs conv. el. (624.15 keV) 2.0 keV for ^{137}Cs gamma (661.6 keV)	*silicon:* X-ray and beta spectrometry (high resolution) *germanium:* gamma ray spectrometry

preamplification: voltage sensitive and charge sensitive, the first having a resistive feedback, and the second a capacitive one (35).

The voltage sensitive preamplifier having the advantage of high signal/noise ratio, presents however a serious problem of stability. As the output pulse height V_0 is given by

$$V_0 = \frac{Q}{C_d}\frac{R_f}{R_k} \tag{6.27}$$

where Q is the collected charge, the pulse height remains dependent on the detector capacitance C_d, which is a function of the applied bias potential. Furthermore the capacitance of the first tube being in parallel with C_d, the temperature of the filament of this tube must be very stable since this affects the space charge around the cathode.

For these reasons, frequent use is made of a charge sensitive or integrating amplifier, where the output pulse height is given by

$$V_0 = \frac{Q}{C_f} \tag{6.28}$$

and is only a function of the feedback capacitance. The use of field effect transistors (FET), which can be mounted in the detector housing and cooled, increases the signal/noise ratio and hence further optimizes the resolution.

The main amplifier, besides providing additional gain, should also control the pulse shape, in order to obtain optimum working conditions. This amplifier has to have the qualities of high stability, extreme linearity and low noise. Sometimes a post amplifier is used, acting as a window amplifier, which enables selection of part of the spectrum. The output of the amplifier can be fed into any single or multichannel analyzer or counting device.

4. *Shielding of Detectors*

Apart from the shielding that must be provided due to the physical properties of the detectors, e.g. screening from light for scintillation detectors, vacuum packing for hygroscopic NaI(Tl) detectors, light shielding, cooling and vacuum packing for some semiconductor detectors, a physical shield should be made to absorb cosmic and other background radiation. As these phenomena constitute the major part of the background, detectors are generally placed in a lead shield

with a thickness of approx. 10 cm. Care should be taken to use lead, free of radioactive fall out products or natural radioactive isotopes. Some typical radioisotopes present in the background of a gamma detector are listed in Table 6.7.

TABLE 6.7
Radioisotopes occurring in the background of a gamma detector (36)

Isotope	Production	Mean energies keV (intensity)	Other energies (keV)
^{40}K	Natural	1460.7 (100)	
^{106}Ru (^{106}Rh)	Fission	511.9(90); 622.3(30); 1050.5(5)	616; 874; 1128; 1061; 1133; 1182; 1195; 1497; 1562; 1767; 1797; 1929; 1989; 2113; 2192; 2239; 2317; 2366; 2390; 2406
^{137}Cs (^{137m}Ba)	Fission	661.6 (100)	—
^{144}Ce (^{144}Pr)	Fission	133.4; 696.4; 2185.8	1488
^{208}Tl	^{232}Th series	583.1; 860.5; 2614.3	278; 511; 763
^{212}Pb	^{232}Th series	238.6	300
^{212}Bi	^{232}Th series	727.3	785; 1078; 1621
^{228}Ac	^{232}Th series	911.0; 968.8; 1583.3	209; 271; 327; 338; 410; 463; 562; 773; 795; 836; 1247; 1460; 1497; 1633
^{210}Pb	^{226}Ra series	46.5	
^{214}Pb	^{226}Ra series	242.0; 295.4; 352.0	258; 274; 481; 534
^{214}Bi	^{226}Ra series	609.3; 768.1; 1120.0	665; 703; 720; 785; 806; 840; 934; 965; 1155; 1207; 1238; 1379; 1386; 1398; 1408; 1510; 1585; 1661; 1731; 1765; 1848; 2110; 2204; 2293; 2447
^{226}Ra	^{226}Ra series	186.2	

Lead shielding with material of recent production will still yield a substantial background due mainly to ^{210}Pb and active daughters. Disintegration rates of ^{210}Pb, ^{210}Bi and ^{210}Po of 100 dpm per gram lead are not unusual (37). Considerable improvement can be achieved with an inner layer of 1 cm thickness of 100 year old lead.

The background of a G.–M. counter is reduced from 80 to 20 cpm by placing the counter in a 5 cm thick lead shield. Whereas the shields of beta detectors are normally of restricted dimensions, as scatter is

not a major problem, the shields of gamma ray detectors are however made as large as possible. Cubic shields of 1 m^3 are not unusual, since scatter of gamma rays on the walls can be important. Moreover the inside is lined with cadmium and copper foil, of about 1 mm thickness, in order to convert the generated 86 keV X-ray of lead to the 12 keV X-ray of copper.

When dealing with the counting of sources of low activity, a further decrease in background may be needed. A G.–M. or proportional counter can be surrounded by a second counter, a so called "guard tube", the signals of the detector being in anticoincidence with the one in the guard tube. A cosmic ray passing through both detectors will not be detected, reducing the background to as low as 1 cpm.

In scintillation counting a purification and selection of the detector materials can reduce the background. NaI(Tl) detectors can be obtained, containing very low ^{40}K concentrations giving a background reduction of a factor 2 over a normal commercial detector.

(B) Alpha Counting

As the problem of alpha detection does not occur frequently in activation analysis, the various possible techniques will be only indicated.

As an alpha particle has a short range, even in air, one always tries to introduce the sample into a gas counter, or to have a vacuum between the detector and the sample.

Therefore an ionization chamber, filled with argon or methane at atmospheric pressure or a windowless or flow proportional counter are suitable. The latter even enables a discrimination between particles of different energies.

A thin slice of a zinc sulphide silver activated crystal or a deposit of this crystal powder on a lucite disc, coupled to a photomultiplier tube provides a simple scintillation counter for alpha particles, and also enables energy discrimination.

By mixing the source material with a liquid or gel scintillator, another detection and discrimination method for alpha rays becomes possible.

The most outstanding detector for spectrometry of alpha particles is the semiconductor detector. A spectrum of the ^{210}Po alpha ray recorded by means of a silicium barrier detector is given in Figure 6.14 (1).

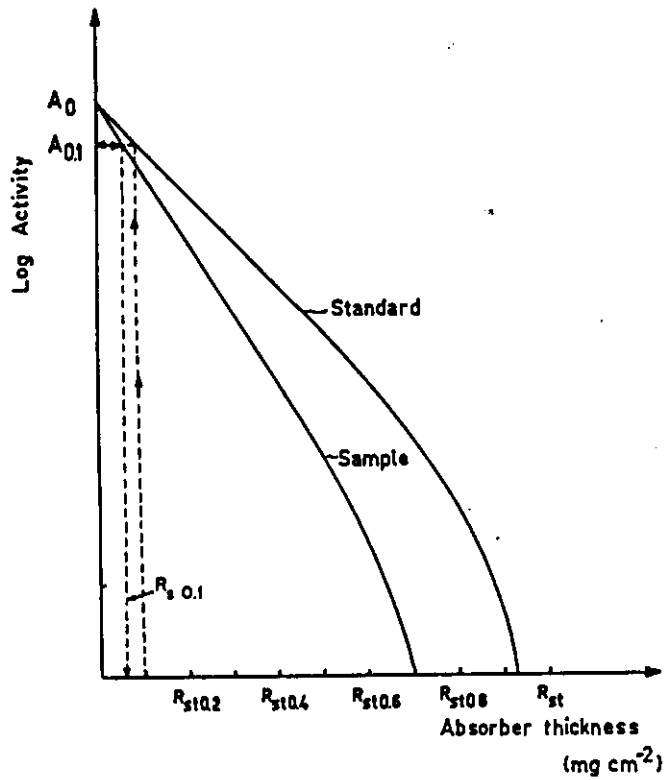

Fig. 6.21. Absorption curve for E_{max} determination of a beta spectrum, according to Feather's method.

(D) Photon Counting

As gamma rays are not easily absorbed, these sources can be counted either in solid form or in solution, which is normally performed using standard counting vials for reproducibility of the geometry. When dealing with X-rays or soft gamma rays, care has to be taken to correct for possible self-absorption and external absorption of the emitted radiation.

The detection of gamma rays is mostly performed by means of a NaI(Tl) scintillator or with a Ge (Li) p.i.n. junction. As the output of these detectors is proportional to the amount of energy absorbed,

integral counting as well as spectrometry is possible. The NaI(Tl) and the Ge (Li) detectors are made in different shapes, according to the purposes for which they will be used. NaI(Tl) is usually made in cylindrical form without or with a coaxial well, the latter allowing the sample to be surrounded by the detector. Dimensions of 7.5 cm × 7.5 cm are commonly encountered, although quite large sizes are available. As sodium iodide is hygroscopic, the crystal is packed in an aluminium can, provided with a MgO or Al_2O_3 reflector to optimize light collection. The crystal is coupled to the P.M. either directly (integral line) or through a thin leucite window. The optical coupling is ensured in the latter case by means of silicon grease.

The Ge(Li) detectors can be made planar, coaxial and U-drifted (34) as can be seen from Figure 6.22.

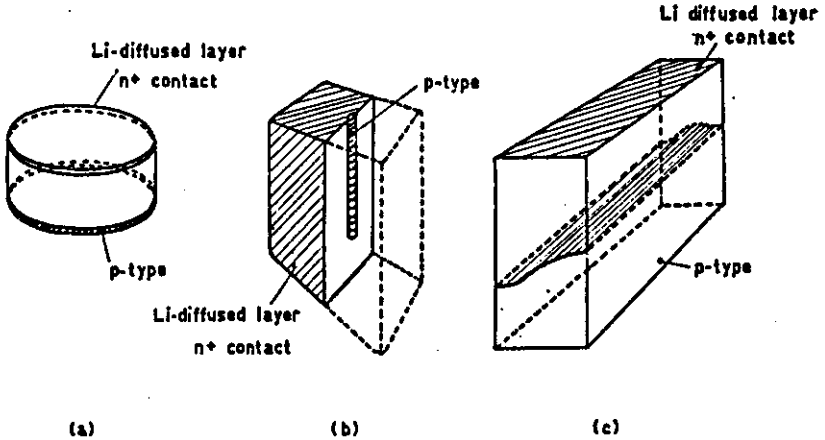

Fig. 6.22. Some typical shapes of Ge(Li) detectors: (a) planar, (b) coaxial, (c) U-drifted (34).

All Ge (Li) detectors have to be cooled with liquid nitrogen and kept under vacuum in order to obtain optimum working conditions. A diagram of a typical detector set up is given in Figure 6.23.

According to the size and the absorbing properties of the detector, and to the energy of the measured gamma ray, total or partial absorption can occur.

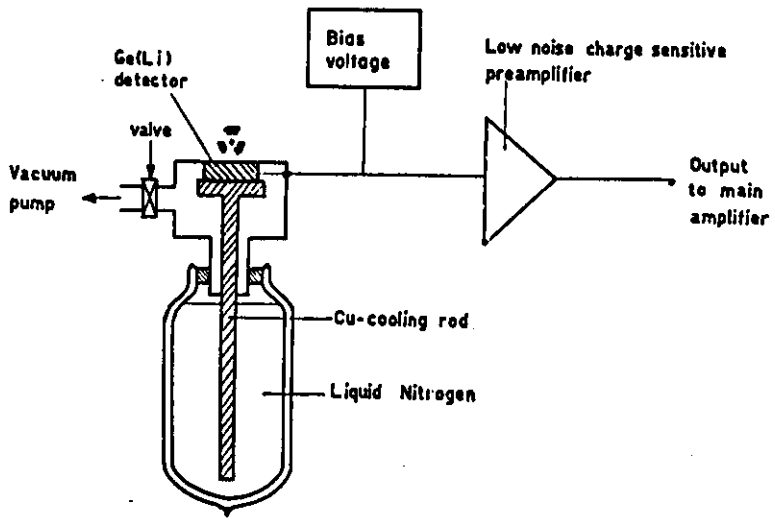

Fig. 6.23. Scheme of a typical Ge(Li) detector mounting.

Total absorption:
- (a) at low gamma energy: photoelectric effect with absorption of the detector X-ray
- (b) at medium gamma energy: successive Compton interaction, ending in a photoelectric absorption
- (c) at gamma energy >1.02 MeV: pair production with total absorption of the positron annihilation quanta, according to (a) or (b).

Partial absorption:
- (d) photoelectric effect, with escape of the detector X-ray
- (e) Compton interaction with escape of the secondary gamma
- (f) pair production with escape of one or both positron annihilation quanta.

Although gamma rays are monoenergetic, it appears that complex spectra are obtained, as is illustrated in Figure 6.24, where the gamma

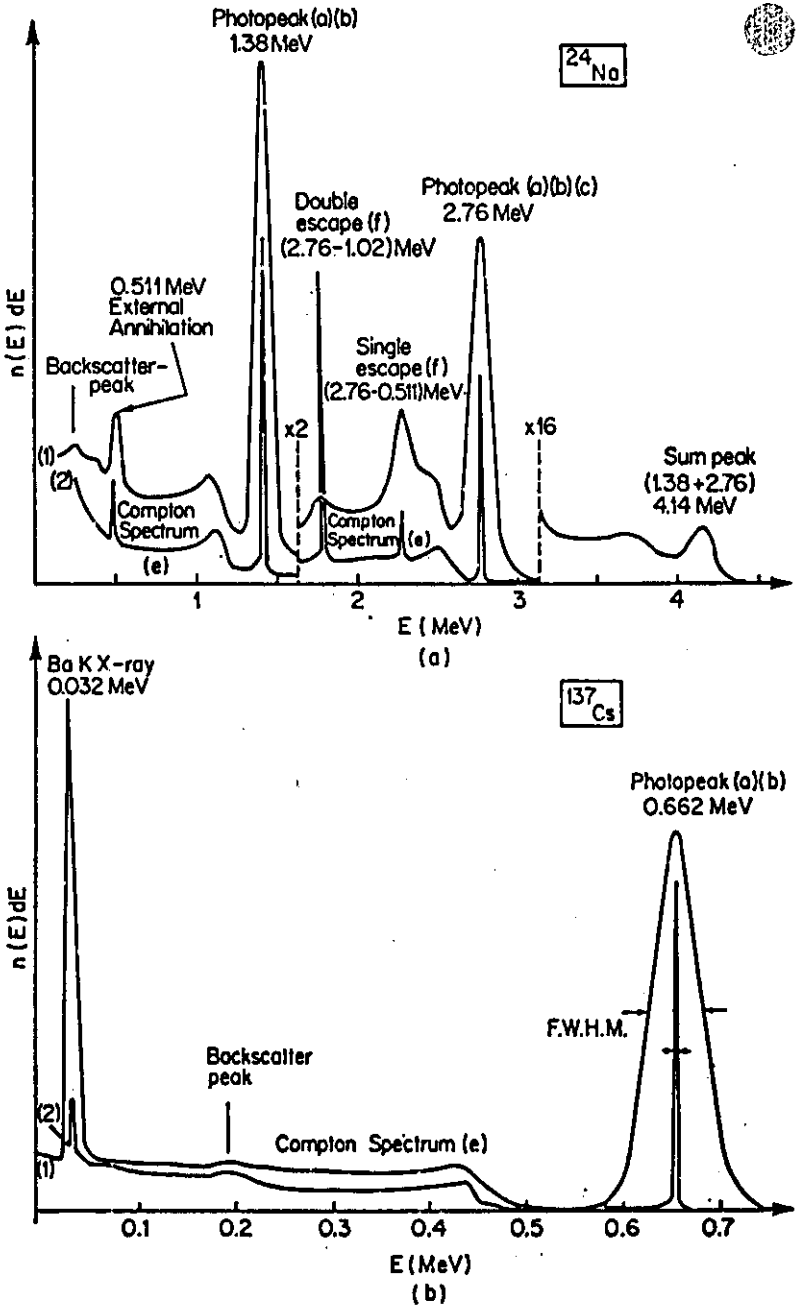

Fig. 6.24. Gamma spectrum of ^{24}Na, ^{137}Cs and ^{170}Tm, measured with a NaI(Tl) (1) and with a Ge(Li) (2) detector.

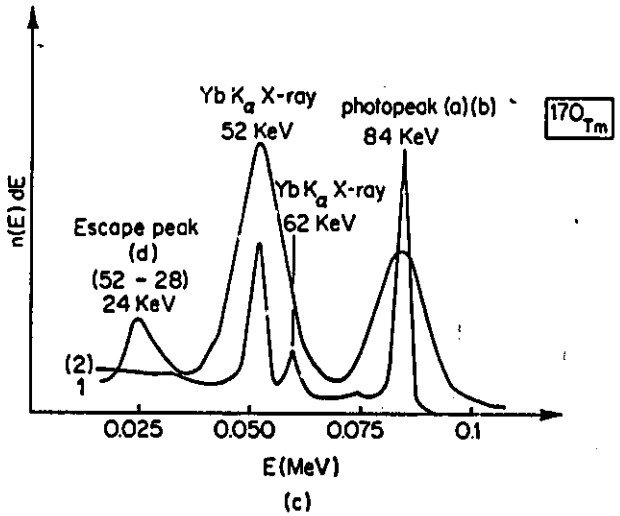

Fig. 6.24. *Continued.*

spectra of ^{24}Na ($E_{\gamma 1}$ = 2.76 MeV; $E_{\gamma 2}$ = 1.38 MeV), ^{137}Cs (E_γ = 0.662 MeV) and ^{170}Tm (E_γ = 0.084 MeV) have been represented for a NaI(Tl) and a Ge(Li) detector.

All processes giving rise to total absorption (a), (b), (c) contribute to the formation of the peak at the highest energy side of the spectrum: the so called photopeak. The Compton interaction with escape of the secondary gamma ray (e) produces the broad Compton spectrum, extending from the Compton edge (equation 6.15) towards energy zero. The escape of the detector X-ray by photoelectric effect (d) accounts for the formation of an escape peak. With NaI(Tl) this peak can be observed at 28 keV (iodine X-ray) below the photopeak when the latter does not exceed ca. 150 keV. At higher energies the escape peak disappears under the photopeak due to the poor detector resolution, and to the reduction in intensity of the escape peak, since the escape probability decreases as the radiation penetrates more deeply into the detector. In Ge(Li) detectors the escape peak should appear at about 10 keV (Ge X-ray) below the photopeak, and should be observed up to energies of approximately 1 MeV. However, the penetrability being higher than in NaI(Tl), and the X-ray energy much smaller, the escape probability is practically negligible, so that escape peaks can hardly be observed.

When dealing with gamma rays with energies higher than 1.02 MeV, single and double escape of the positron annihilation quanta (f) produce peaks at energies respectively 0.511 and 1.02 MeV below the gamma ray energy. In this case an annihilation peak also occurs at 0.511 MeV due to positron escape and subsequent annihilation in the surrounding materials (external annihilation).

When positron emitters are measured, the typical annihilation gamma ray of 0.511 MeV appears in the spectrum, and in good geometry also the 1.02 MeV sumpeak. Indeed, the possibility always exists that two or more gamma rays coincide in the detector, giving rise to a sumpeak. The relative intensity of the sumpeak to the single peak will be a function of the source detector geometry.

Beta emitters give rise to a Bremsstrahlung spectrum, starting at the E_{max} of the beta ray and increasing in intensity towards lower energies. The gamma rays of the source can also give rise to Compton scattering with the surrounding materials, whereby the gamma rays are reflected over about 180° before they reach the detector. This gives rise to a broad backscatter peak, with a maximum at about 250 keV, as can be calculated from equation (6.13). To reduce this effect large lead shields are recommended, removing in this way all materials as far from the detector as possible. For the same reason, sample holders etc. are made from low Z plastic materials.

When X-rays or gamma rays below 100 keV are to be measured, a Si(Li) detector, a proportional gas counter, or even a NaI(Tl) wafer are preferred over the conventional gamma ray detectors. The wafer detector consists of an extremely thin NaI(Tl) crystal, giving rise to low efficiency for gamma rays over 100 keV as can be seen from Figure 6.25 where the detection efficiencies for a wafer of 7.5 cm diameter by 0.10 cm thickness, covered with a 37 mg/cm² beryllium window are given (56).

From Figure 6.25 it appears that X-rays and low energetic gamma rays can be measured with a wafer detector, with greatly reduced interference of the Compton spectrum of higher gamma energies.

In order to achieve gamma spectrometric measurements, pulse height discrimination becomes necessary, which can be done either with a single channel or a multichannel pulse height analyzer. A single channel analyzer consists in principle of a double discrimination circuit, the outputs of which are fed into an anticoincidence unit, as can be seen from Figure 6.26. In this way only pulses having an amplitude between

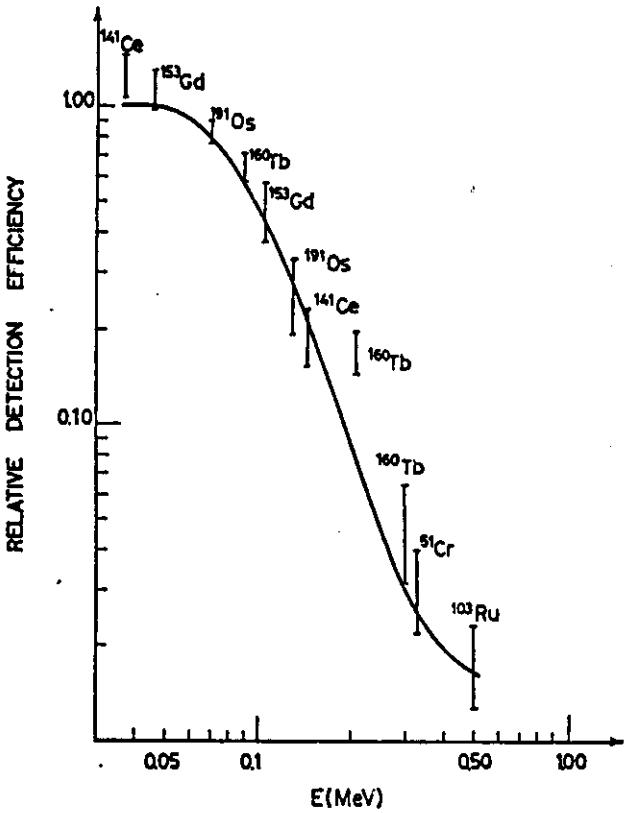

Fig. 6.25. Calculated photopeak detection efficiency ratio for a NaI(Tl) wafer of 7.5 cm diameter × 0.1 cm thickness, provided with a 37 mg cm^{-2} beryllium window to a 7.5 × 7.5 cm NaI(Tl) detector (56).

V and $V + \Delta V$ are allowed to pass through the analyzer. V is called the threshold or bias tension, whereas ΔV is called the window width.

To obtain the whole spectrum, the pulse height scale has to be scanned step by step, using a digital counter, or continuously, using a ratemeter and a recorder. A window of about 1% of the full threshold value should be used in order to obtain good spectrum resolution, whereas part of the spectrum (e.g. a photopeak) can be selected by means of an appropriate bias and window setting.

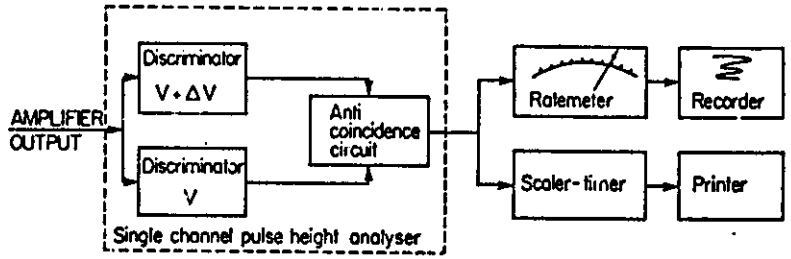

Fig. 6.26. Scheme of a single channel analyzer and related equipment.

An advantage of the single channel analyzer is that the dead time of the circuitry is low (order of the μs) and constant.

In the multichannel analyzer use is made of an analogue to digital converter (A.D.C.) and a ferrite memory block in order to allow the simultaneous measurement and storage of pulse amplitudes. A block-diagram of such an apparatus, with auxiliary output equipment is shown in Figure 6.27. With NaI(Tl) detectors, 400 channel memories are typical, whereas Ge(Li) detectors require at least 2000 channels for efficient use of the high resolution.

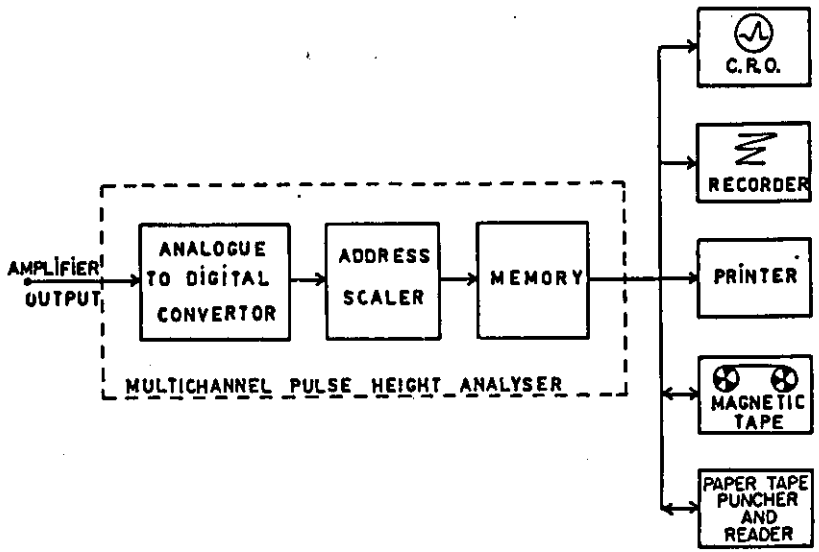

Fig. 6.27. Scheme of a multichannel analyzer and related equipment.

The use of an A.D.C. implies however an appreciable dead time of the apparatus, depending on the A.D.C. oscillator frequency and the read-in time of the analyzed pulse in the memory block. In this way the dead time per count τ_i for the i^{th} channel is given by:

$$\tau_i = k_1 + k_2 i \tag{6.36}$$

where k_1 is a constant, due to memory-cycle storage time and k_2 another constant, depending on the oscillator frequency. However, an electronic correction circuit (live timer) stops the timer during the pulse height analysis. The live timer thus indicates true counting duration.

The limitations of automatic dead time correction are discussed in Chapter 10.

The use of transistors and integrated circuits reduces the dimensions of this rather complex equipment to quite small sizes. It is obvious that high stability and low noise are the first requirements for all spectrometric apparatuses, which implies that only high quality components can be used. In addition, the use of a thermostatized counting room is recommended, as detectors and electronics are sensitive to temperature changes. In order to minimize shifts of gain or base line origin, several spectrometer stabilizers have been described, which operate through a feedback circuit to the detector high voltage or to the amplifier gain. A measured photopeak (57,58,59) can be used as a reference peak, or an electronic reference pulse can be generated by means of a pulse generator (60) or a flashlight on the P.M. (61). Covell (62) proposed a procedure for quality control of long-term stabilized instrumentation. A standard spectrum is periodically measured and compared with a reference spectrum, on a channel-by-channel basis by means of a computer.

Possibility of negative or positive storage in the multichannel analyzer enables background correction and spectra subtraction, as is often done in the spectrum stripping method (Chapter 9, section III, A).

Half lives of isotopes can be followed by using each channel as a separate counter in the multiscaler operation mode. A clock controls counting time and channel advance, whereas energy discrimination remains possible by means of an external or internal single channel analyzer.

The resolution of a gamma spectrometer varies with the gamma ray energy, and is normally given for the 0.662 MeV peak of ^{137}Cs. With a NaI(Tl) detector, the resolution R is expressed in percent, using the

ratio of the full width at half maximum (FWHM) of the photopeak, to the peak energy E, as can be seen from Figure 6.24:

$$R(\%) = \frac{(\text{FWHM})100}{E} \tag{6.37}$$

Resolutions between 7 and 10% are normally encountered depending on the quality of the crystal and the P.M. The contribution of both crystal and P.M. to the resolution of the detector is energy dependent. The resolution of the P.M. (R_p) in percent is given by Hickok and Draper (63) as follows:

$$R_p^2 = k_1 + k_2 E^{-1} \tag{6.38}$$

whereas Kelley *et al.* (64) found that the crystal resolution (R_c) could be represented by:

$$R_c^2 = k_3 E^{-1/2} \tag{6.39}$$

where k_1, k_2 and k_3 are constants depending on the apparatus and E is the gamma energy.

Combining equations (6.38) and (6.39) yields for the total detector resolution (R):

$$R^2 = R_p^2 + R_c^2 = k_1 + k_3 E^{-1/2} + k_2 E^{-1} \tag{6.40}$$

Experiments performed by De Soete and Hoste (65) confirmed this relationship, and demonstrated that in the region between 100 keV and 2 MeV, the parabola in $E^{-1/2}$ of equation (6.40) practically coincides with a straight line, so that one can write:

$$(R^2)_{0.1-2\,\text{MeV}} = k + k' E^{-1/2} \tag{6.41}$$

where k and k' are apparatus constants. Equation (6.41) provides an easy way to obtain the detector resolution as a function of energy, which can be important for computer analysis of complex gamma spectra. As the resolution of a NaI(Tl) detector is of the order of 10%, the line broadening due to noise in the electronic circuits can be neglected. The spectrometer resolution is thus given by the detector resolution.

When dealing with Ge(Li) detectors, the resolution is normally expressed as the FWHM in keV of the 0.662 MeV ^{137}Cs peak. Typical resolutions for this type of detectors are between 5 and 2 keV, resulting in an improvement of a factor 10 to 20 in comparison with NaI(Tl) detectors.

Here again, the detector resolution (R_D) is energy dependent, and can be expressed as follows:

$$R_D^2 = 2.355\, FE\epsilon \tag{6.42}$$

where R_D and the gamma energy, E, are expressed in keV and ϵ is the energy needed to create an electron–hole pair and is approximately equal to 3.10^{-3} keV for Ge. The Fano factor F (variance-to-yield factor) is 0.129 with the Ge(Li) detector at liquid-nitrogen temperature (66,67,67a). It is obvious that with this type of detector the electronic line broadening plays an important role. The resolution of the spectrometer (R) is therefore composed of the electronic line broadening (R_E) and of the detector resolution (R_D):

$$R^2 = R_E^2 + R_D^2 \tag{6.43}$$

The main factor inducing electronic line broadening is the noise produced by the detector surface leakage current and by the amplifying equipment. The electronic noise of the spectrometer is readily determined by measuring the distribution of a pulse amplitude, produced by a stable pulser.

From equation (6.42) one can calculate that the detector resolution of a 100 keV photopeak should be about 0.4 keV, so that in this energy region the electronic broadening will dominate. Preamplifier design is making rapid progress to produce equipment with extremely small electronic line-broadening.

Using a Ge(Li) detector, one can observe that the 0.511 MeV positron annihilation photopeak usually has a broader resolution than a gamma ray of the same energy. This could be explained by Doppler broadening, due to the fact that annihilation occurs when the positron electron pair has a kinetic energy different from zero.

In comparison with the sodium iodide crystals, the main disadvantage of the Ge(Li) detectors is their lower photopeak efficiency. Actually, however, sizes up to 100 cm³ sensitive volume are possible, increasing the photopeak efficiency, as can be seen from Figure 6.23.

The photopeak efficiency is a function of the intrinsic detector efficiency, which depends on the gamma energy and the source–detector geometry, and on the peak/total ratio. This is the ratio of the activity measured under the photopeak to the total activity of the spectrum. Intrinsic efficiencies and peak to total ratios for a 7.5 cm ×

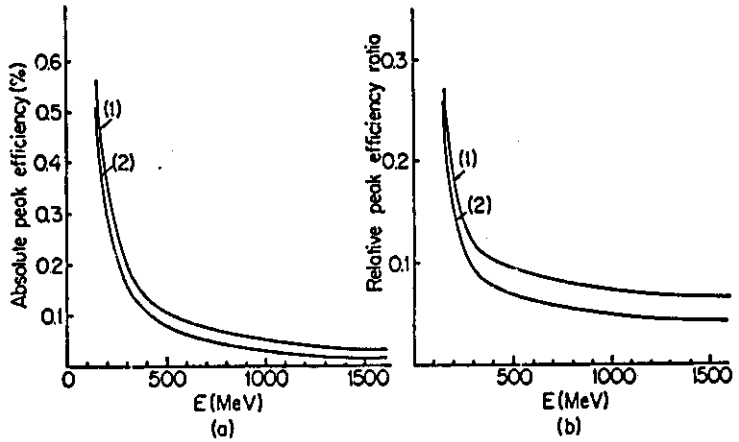

Fig. 6.28. Photopeak efficiency for a 40 cm³ (1) and a 18 cm³ (2) Ge(Li) detector: (a) absolute, (b) relative to a cylindrical 7.5 cm × 7.5 cm NaI(Tl) detector (34).

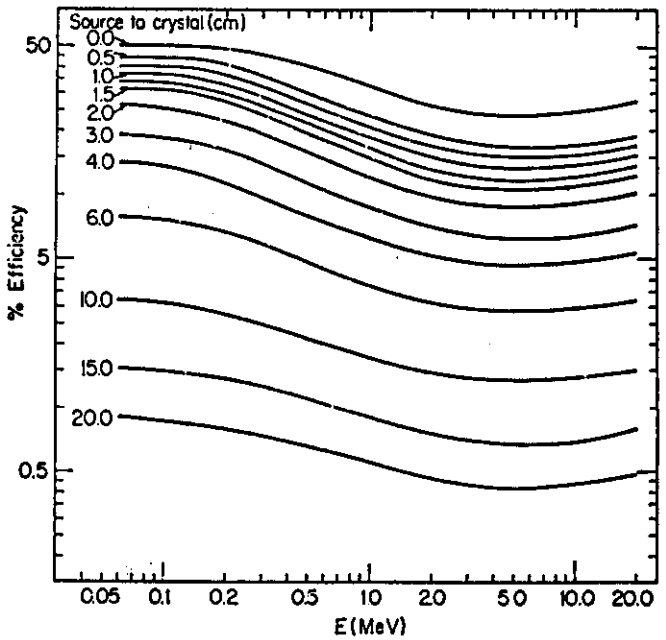

Fig. 6.29. Point source efficiencies for a 7.5 cm × 7.5 cm cylindrical NaI(Tl) detector, as a function of gamma energy and source–detector distance (69).

7.5 cm NaI(Tl) detector and a point source are given in Figures 6.29 and 6.30 and can be obtained from the literature (68,69,70).

For Ge(Li) detectors the calculation of these data becomes very difficult, as the efficiency varies practically for each detector.

The energy of the unknown gamma ray can be determined from the pulse height of the photopeak maximum. The calibration of the spectrometer is performed by means of isotopes emitting gamma rays of known energies. Sets of calibration sources are commercially available or can be prepared by irradiation of the stable isotopes. As a

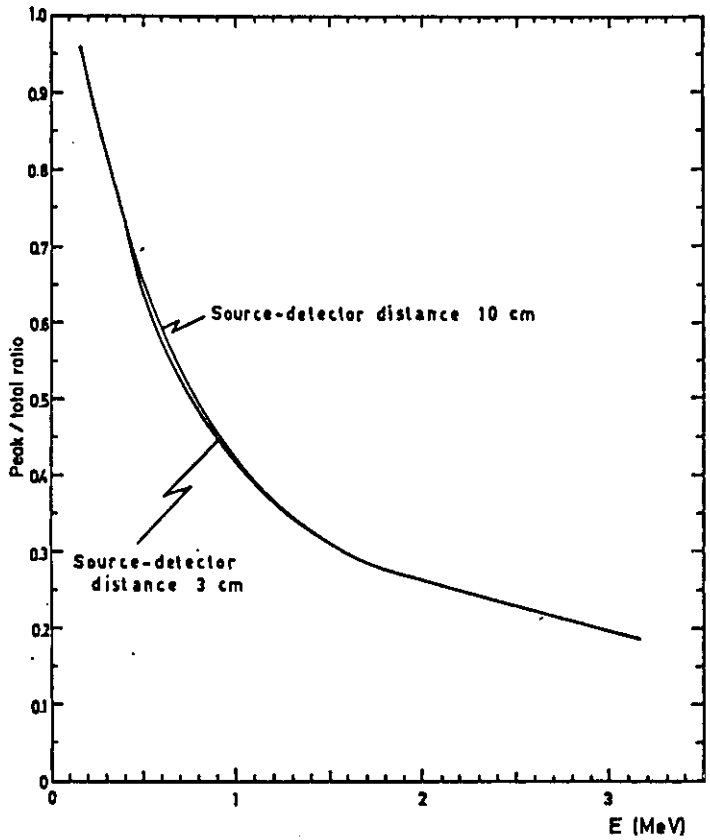

Fig. 6.30. Experimental peak-to-total ratios for a 7.5 cm × 7.5 cm cylindrical NaI(Tl) detector, as a function of gamma energy, and source–detector distance (68).

Ge(Li) detector shows a very good resolution, gamma ray energies can be determined within a few tenths of a keV. This implies an accurate knowledge of the energies of the calibration sources, a list of which is given in Table 6.11.

Catalogues of gamma ray spectra measured with NaI(Tl) and Ge (Li) detectors are also very helpful for the identification of gamma spectra (68,69,71,72,73,74). With Ge(Li) detectors, the problem occurs of the nonlinearity of practically all A.D.C. circuits, resulting in nonlinear calibration curves. To minimize errors of this kind it is recommended to calibrate the apparatus in the region where the unknown peak occurs, instead of using an overall calibration curve.

Quantitative data of the gamma ray intensity can be obtained from the area or the height of the photopeak. Indeed, as the line broadening

TABLE 6.11
Calibration sources for gamma ray spectrometry (36)

Isotope	Energy (keV)	Isotope	Energy (keV)
^{241}Am	59.568 ± 0.017	^{95}Nb	765.83 ± 0.07
^{131}I	80.166 ± 0.009	^{54}Mn	834.84 ± 0.07
^{153}Gd	97.43 ± 0.02	^{88}Y	898.01 ± 0.07
^{153}Gd	103.18 ± 0.02	^{207}Bi	1063.82 ± 0.28
^{177}Lu	112.97	^{60}Co	1173.13 ± 0.04
^{141}Ce	145.44 ± 0.05	^{60}Co	1332.39 ± 0.05
^{139}Ce	165.84 ± 0.03	^{24}Na	1368.40 ± 0.04
		^{56}Co(D.E.)	1576.9 ± 0.32
^{177}Lu	208.36	^{208}Tl(ThC″)(D.E.)	1592.3 ± 0.13
^{203}Hg	279.12 ± 0.05	^{24}Na (D.E.)	1731.6 ± 0.16
^{131}I	364.47 ± 0.005	^{88}Y	1836.1 ± 0.07
		^{56}Co	2035.2 ± 0.50
		^{56}Co(D.E.)	2232.2 ± 0.67
^{198}Au	411.776 ± 0.01	^{24}Na (S.E.)	2242.6 ± 0.14
		^{56}Co	2598.9 ± 0.30
Annihilation	511.006 ± 0.02	^{208}Tl (ThC″)	2614.3 ± 0.09
^{207}Bi	569.65 ± 0.10	^{24}Na	2753.6 ± 0.12
^{137}Cs	661.59 ± 0.07	^{56}Co	3202.4 ± 0.65
		^{56}Co	3254.2 ± 0.65
		^{56}Co	3273.6 ± 0.4
		^{56}Co	3452.5 ± 0.75

S.E. = single escape D.E. = double escape.

is a statistical phenomenon, the photopeak can be described as a Gaussian error curve, with an area S, given by

$$S = 1.06(\text{FWHM})h \tag{6.44}$$

where h is the peak height. The peak height can be measured after recording or drawing the spectrum, or by taking the number of counts in one or more channels in the peak top. However, when peaks are superimposed on the Compton continuum of higher energy gammas, or when poor counting statistics are obtained, which is often the case in trace analysis, the determination of the peak height becomes very difficult. An estimation of the Compton background has to be performed, which is in most cases troublesome and inaccurate.

Using equation (6.44) Connally and Leboeuf (75) calculated peak areas by measuring h and reading the FWHM from a calibration curve. It is evident that here again the problem of the Compton background remains unsolved. The simplest way to correct for Compton interference is to draw a straight or a curved line across the bottom of the peak, as represented in Figure 6.31(a) and planimetry of the thus obtained area. This method is only approximate and can give rise to quite large errors, when the peak is superimposed on a Compton edge. A method, similar to the one described by Connally *et al.* is proposed by McIsaac (76) and is shown in Figure 6.31(b). Graphically the point is determined where the photopeak width equals the FWHM and the area above this point is found by planimetry. When the height of the peak above FWHM is measured, the true photopeak height is the double of this value, and the peak area can be calculated by means of equation (6.44).

When dealing with a multichannel analyzer where the spectrum is present in a digital form, the method which is mostly used to determine the peak area is due to Covel (77), as represented in Figure 6.31(c). The channel with the highest activity A_0 is determined and called n_0. Symmetrically on both sides of n_0 one takes an equal number of channels, in such a way that the activity A_l and A_m in channel n_l and n_m is somewhere between A_0 and the activity in the minima at both sides of the peak. The activity A of the area above the line $n_l - n_m$, which is proportional to the total peak area, can be calculated as follows:

$$A = \sum_{n=n_l}^{n=n_m} A_n - (n_m - n_l)\frac{(A_l + A_m)}{2} \tag{6.45}$$

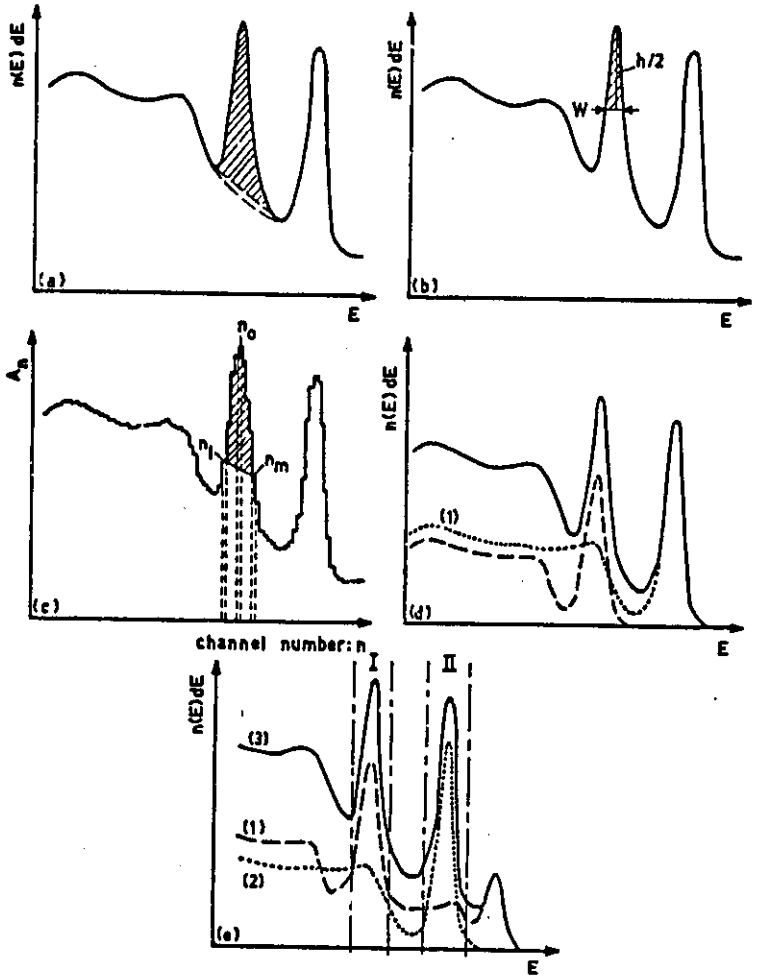

Fig. 6.31. Determination of the photopeak area in a complex gamma spectrum.

This technique is very rapid and gives excellent results with both NaI(Tl) and Ge(Li) detectors.

A widely used technique to correct for the interaction of higher energy gammas on lower energy photopeaks is the spectrum stripping method as represented in Figure 6.31(d). From the complex spectrum a pure spectrum of the highest gamma energy (1) is subtracted either graphically, by means of the multichannel memory or even by a com-

puter. In this way, the lower energy photopeak is obtained free of interferences.

Care should be taken that standard spectra and samples are measured exactly in the same geometrical conditions and have about the same count rate. Furthermore gain shifts can introduce serious errors. The technique can be repeated subsequently for the highest peak in the new spectrum in order to determine lower photopeaks. One should bear in mind that each subtraction implies increased statistical errors, limiting in this way the number of possible subtractions.

Another method which can be used is the gamma spectrometry in broad channels, as is shown in Figure 6.31(e). When two isotopes, having respective spectra (1) and (2), are present in a sample, a complex spectrum (3) is obtained. From the measurement of the activity in channels I and II of the pure isotopes and of the mixtures, the contribution of spectrum (1) in channel I ($A_{(1)I}$) and of spectrum (2) in channel II ($A_{(2)II}$) can be computed as follows:

$$A_I = A_{(1)I} + A_{(2)I}$$
$$A_{II} = A_{(1)II} + A_{(2)II} \qquad (6.46)$$

where A_I and A_{II} are the activities of the complex spectrum in channel I and II respectively, $A_{(2)I}$ is the contribution of spectrum (2) in channel I and $A_{(1)II}$ is the contribution of spectrum (1) in channel II. The ratios $k_{(1)}$ and $k_{(2)}$

$$k_{(1)} = \frac{A_{(1)II}}{A_{(1)I}} \quad \text{and} \quad k_{(2)} = \frac{A_{(2)I}}{A_{(2)II}} \qquad (6.47)$$

can be determined by means of the pure spectra (1) and (2). Substitution of (6.47) in (6.46) yields

$$A_I = A_{(1)I} + k_{(2)}A_{(2)II}$$
$$A_{II} = k_{(1)}A_{(1)I} + A_{(2)II} \qquad (6.48)$$

which is a set of two equations with two unknowns, and thus can be easily solved. In principle this method is not limited to two components, but can be extended to n components, and the obtained set of n equations with n unknowns can be solved by matrix inversion. Here again the aid of a computer becomes desirable. Sample and standards should be measured with the same precautions as described in the spectrum stripping method.

A source of errors one can never avoid, is the formation of random sumpeaks, which are absent in the standard spectra. This effect becomes important at high count rates and in high geometries (e.g. a well detector).

The qualitative and quantitative interpretation of complex gamma spectra, which is generally quite time consuming, can be simplified by computer techniques (78,79,80,81). It is indeed possible to feed the A.D.C. data directly to an on-line computer or to transfer the multichannel memory data to computer compatible magnetic or punched tape. A suitable program allows the smoothing of the spectra, to minimize the influence of the statistical counting fluctuations. First and second derivatives of the spectrum detect the location of the photopeaks. The net photopeak area can subsequently be found by numerical integration after spectrum decomposition or simply by Covells method. Gain shifts between sample and standard can even be corrected for, whereas composite photopeaks can be analyzed into their components. The quantitative analysis of the sample by comparison with the standards can be performed by means of a least squares method (82), which also allows the calculation of the statistical error.

When measuring large samples one has to take into account that attenuation of the gamma rays in the sample and scatter can cause significant errors, as is described in Chapters 7 and 10.

(E) Special Counting Techniques

In order to avoid or to minimize chemical separations, special counting techniques are sometimes used, which are intended to be selective for a given isotope. In gamma ray spectrometry photopeaks of lower energies are often superimposed on the Compton spectrum of higher energies. Although Ge(Li) detectors allow rather easy unscrambling of complex spectra, half-life determination coupled with energy selection, coincidence techniques and Compton compensation methods are used. Half-life measurements can be performed with any counting equipment and will therefore not be discussed separately in this chapter. Some examples of this method are given in Chapter 9, section II, A2.

1. *Coincidence Techniques*

As the nuclear disintegration is characteristic for a given isotope, specific measurements can be performed by means of coincidence techniques, whereby correlated phenomena must be simultaneously detected in order to be counted. As well beta–gamma as gamma–gamma cascades of the disintegration, which occur within very short time intervals, are suitable for these purposes. Also both annihilation gamma rays can be measured in coincidence.

A schematic drawing of a two channel "slow" coincidence system and a two channel "fast–slow" coincidence system is given in Figures

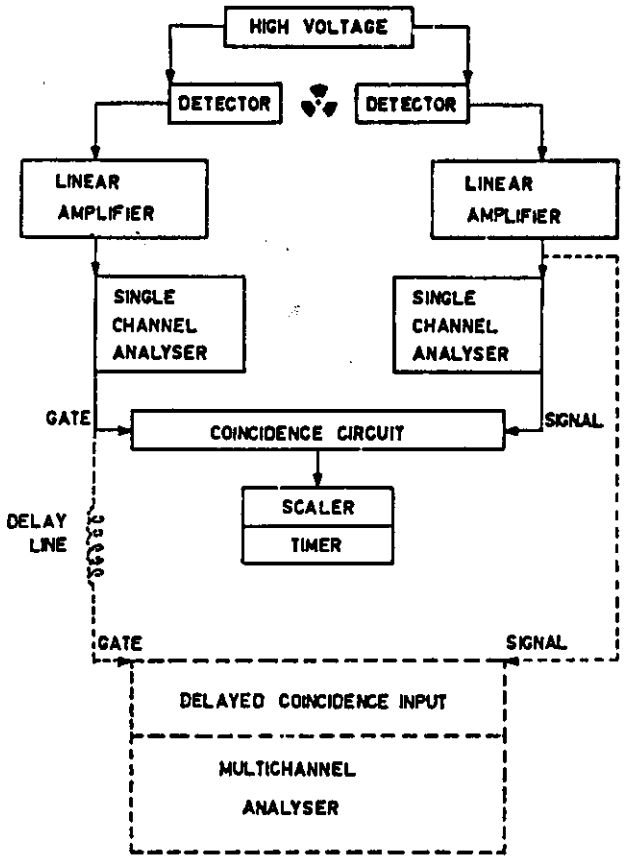

Fig. 6.32. Principle diagram of a "slow" coincidence spectrometer.

6.32 and 6.33. In this set up two detectors are used, a beta detector and a gamma detector for the beta–gamma coincidence measurements and two gamma detectors for the gamma–gamma coincidence.

The pulses coming from the components of the cascade can be selected in energy by means of a pulse height analyzer, and are fed into the coincidence circuit, one providing the gate pulse and the other one the signal pulse. In order to be counted, two pulses must arrive within the resolving time τ of the coincident unit. Typical values of τ are of the order of the μs for "slow" coincidence and down to the ns for "fast" coincidence. Adequate delay lines compensate for the time difference obtained in the two channels. Most multichannel analyzers have built in "slow" coincidence possibilities, giving the advantage

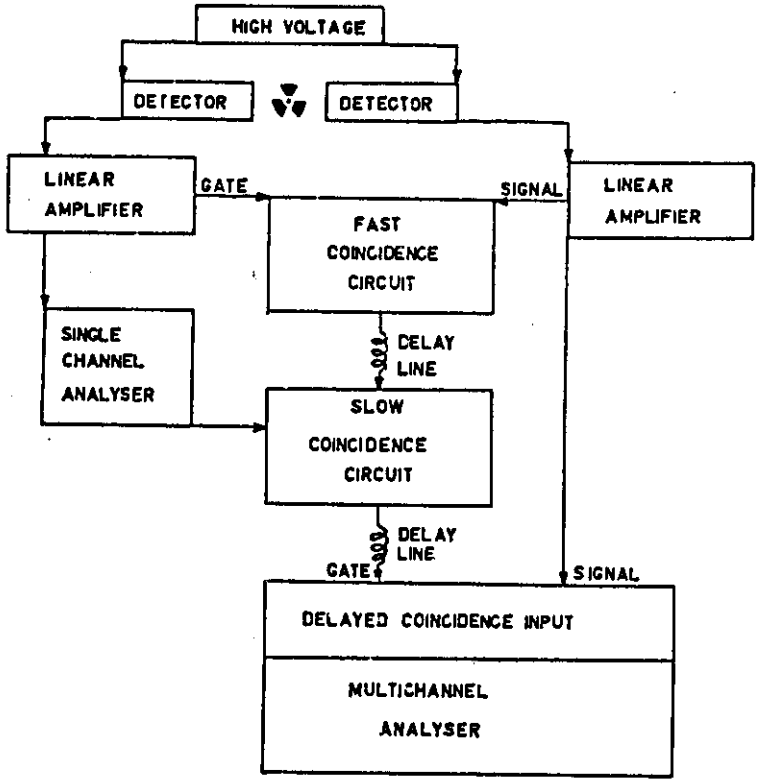

Fig. 6.33. Principle diagram of a "fast–slow" coincidence spectrometer.

that the coincidence spectrum can be visualized. In "fast" coincidence frequent use is made of amplifiers, providing bipolar pulses, to time the coincidence unit at the cross-over point of the pulse. Unfortunately in most amplifiers the cross-over point is a function of the pulse amplitude, causing unwanted jitter, and hence broadening of the resolving time. In an alternative mode of operation the logic output signals are time-referenced to a signal derived from the leading edge of the input signal. In that case the time shift of the output pulse depends mainly on the rise time of the input pulse.

A modification of a coincidence spectrometer, using a dual channel and a multichannel analyzer is described by Johnson (83). In this technique, not only the signal pulses, but also the gate pulses are stored in the coincidence spectrum. This gives rise to better statistics, since the activity due to both components of the cascade can be summed from the spectrum stored in the multichannel memory.

The true coincidence count rate R_c for a source with a disintegration rate D is given by:

$$R_c = Dz_1z_2 \tag{6.49}$$

where z_1 and z_2 represent the respective counting efficiencies of the channels.

At any count rate, a random coincidence count rate R_r occurs, which is given by:

$$R_r = 2\tau R_1R_2 \tag{6.50}$$

where R_1 and R_2 represent the count rates in the respective channels. Taking into account:

$$R_1 = Dz_1 \quad \text{and} \quad R_2 = Dz_2 \tag{6.51}$$

one obtains:

$$R_r = 2\tau D^2z_1z_2 \tag{6.52}$$

From equations (6.49) and (6.52) it appears that at high count rates R_r becomes important, since it varies with D^2, whereas the true coincidence rate is linear with D. As R_r is on the other hand a function of τ and R_c is independent of τ, the "fast–slow" coincidence technique makes a preselection of the coincident pulses at the output of the linear amplifiers, where resolving times can be achieved of about two orders of magnitude smaller than in "slow" coincidence.

From equation (6.49) it is obvious that the detection efficiency of a coincidence system is lower than that of a classical gamma spectrometer. The improvement in the signal to background ratio however largely compensates for this inconvenience. A background of 0.3 cpm for a resolving time of 0.2 μs can easily be obtained. As an example, a spectrum of a 1 g irradiated bismuth sample, containing 0.226 ppm copper is shown in Figure 6.34 with and without coincidence measurement. The 0.511 MeV annihilation peak of ^{64}Cu cannot be detected in the ^{210}Bi Bremsstrahlung spectrum when no coincidence technique is applied.

When gamma cascades are available, the sum coincidence technique developed by Hoogenboom (85) can be applied (86). The apparatus is schematically given in Figure 6.35, together with a sum-spectrum of ^{124}Sb.

The sum of the signals of two NaI(Tl) detectors is made after linear amplification. The sumpeak, produced by total absorption of both cascade gamma rays is selected from the sum spectrum by means of a pulse height analyzer, and used as a gate pulse for the signal of one of the detectors. With this technique, which gives rise to a very low background (0.3 cph), net photopeaks are obtained. Although normally only two cascade gamma rays are measured, theoretically the method can be extended to more than two components of a cascade. A separate detector is however needed for each gamma ray that is intended to be measured, which causes a practical limitation.

An improvement in resolution is also obtained, as the resolution of the photopeaks in the sum spectrum, R_{1s} and R_{2s}, are given by:

$$R_{1s} = R_{2s} = \frac{R_1 \times R_2}{R_1^2 + R_2^2 + R_s^2} \tag{6.53}$$

where R_1, R_2 and R_s are respectively the resolutions of the two cascade photopeaks and the sum peak in the normal spectrum.

The detection efficiencies of the cascade gammas in the sum spectrum z_{1s} and z_{2s}, are given by

$$z_{1s} = z_{2s} = 2\left(\frac{\ln 2}{\pi}\right)^{1/2} z_1z_2 \frac{R_s}{R_1^2 + R_2^2 + R_s^2} \tag{6.54}$$

where z_1 and z_2 represent the efficiencies in the normal spectrum. It has to be noticed however that this method is more subject to random coincidences caused by interferences than the gamma–gamma coincidence method. A study of the applicability of coincidence techniques in activation analysis has been published by Schulze (87).

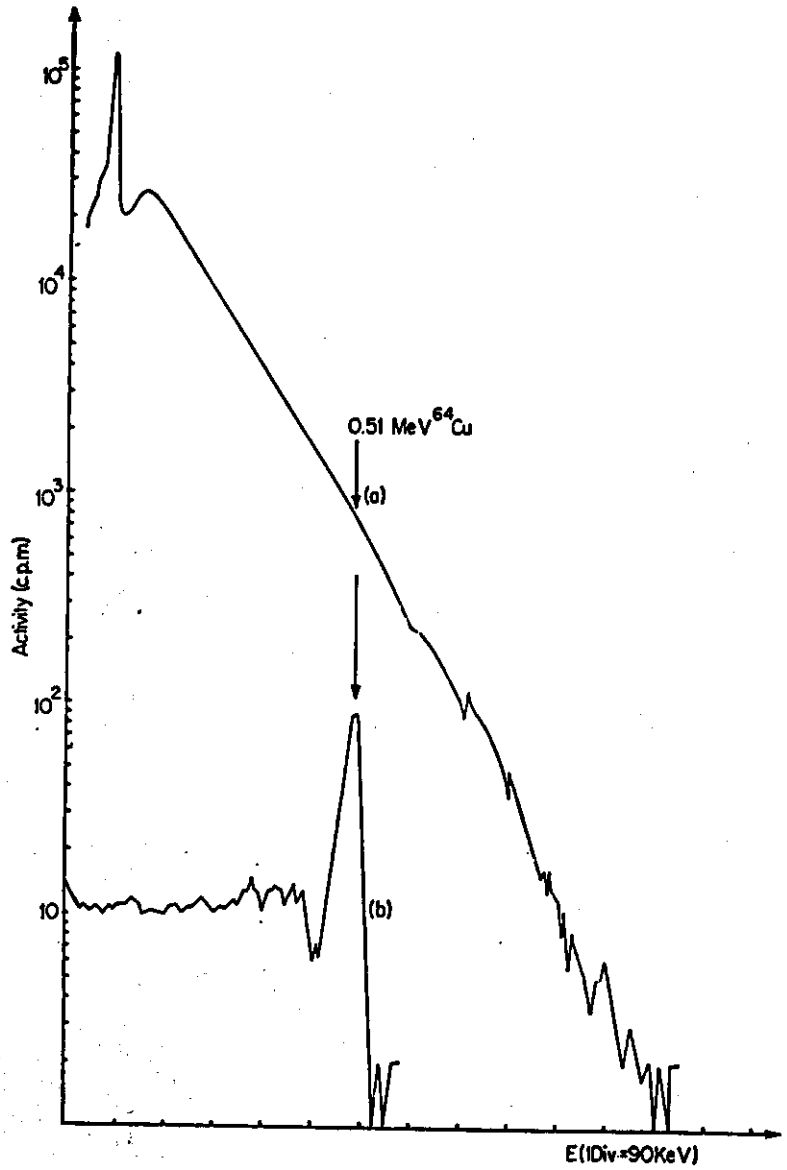

Fig. 6.34. Gamma spectrum of the ^{64}Cu annihilation radiation with the Bremsstrahlung spectrum of ^{210}Bi, measured without (a) and with (b) a coincidence technique in a neutron irradiated 1 g Bi sample, containing 0.226 ppm Cu (84).

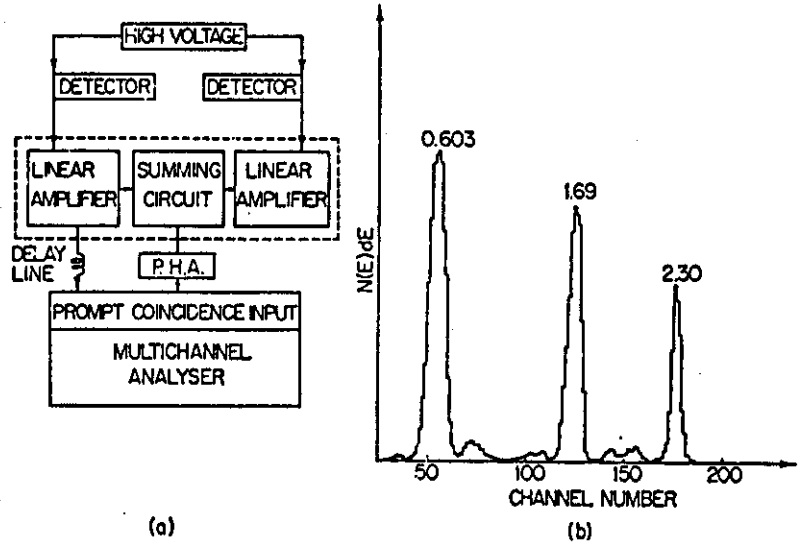

Fig. 6.35. Principle diagram of a two channel sum-coincidence spectrometer (a), and the sum-coincidence spectrum of ^{124}Sb (b).

2. *Compton Compensated Methods*

Compton compensation methods can be divided into two groups: the anticoincidence techniques and the Compton subtraction techniques.

In the anticoincidence techniques (88,89,90,91), use is made of a central detector surrounded by a second annular detector, the signals of both being put in anticoincidence. The escaping secondary gamma of a Compton interaction in the main detector is measured in the annular detector, and hence the circuit prevents the storage of this interaction. By this method a gamma spectrum in the main detector is obtained showing a reduction in Compton background of about 70%. The annular detector can be a large NaI(Tl) crystal, an organic plastic scintillator, or even a tank with liquid scintillator. A schematic representation of the apparatus is shown in Figure 6.36.

A promising anti-Compton device has been described recently by Palms *et al.*, (92,93,94) consisting of a concentric duode Ge(Li) sum spectrometer. As can be seen from Figure 6.37, where a scheme of the apparatus is shown, the detector is made from a single *p*-type Ge

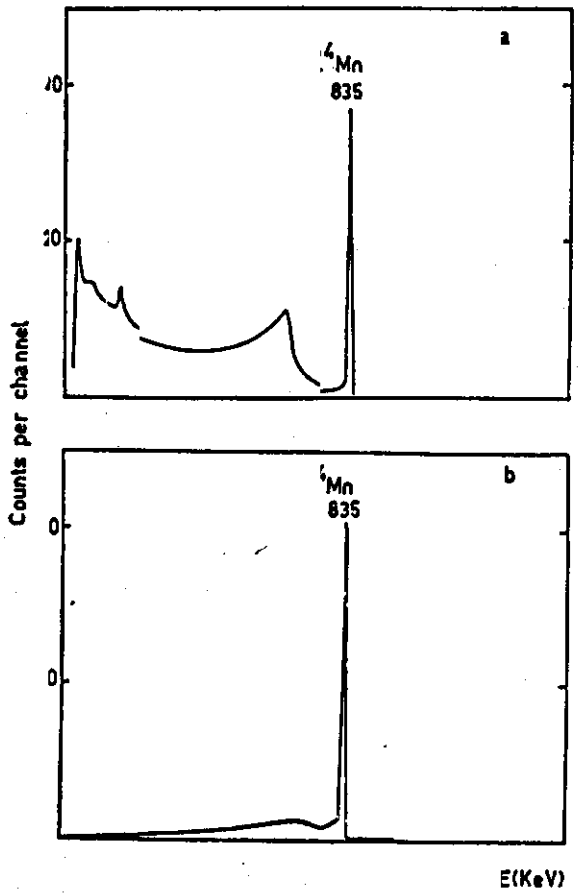

Fig. 6.38. Spectrum of ^{54}Mn measured with a Ge(Li) concentric diode (92).
Curve a: measured as the sum of two separate coaxial detectors.
Curve b: measured in the sum coincidence mode.

R_P represents the detector contribution to the resolution of the poorest detector and $R_{T,E}$ the total electron resolution of both devices. It is obvious that the resolution depends strongly on the perfect gain matching of both detector chains before the input of the summing amplifier which is the last stage of one of the amplifiers.

In the Compton subtraction method the Compton background of a spectrum taken with a NaI(Tl) detector is subtracted by means of a second detector giving rise to Compton background only. For this purpose anthracene can be used, as proposed by Peirson (98,99) although an organic plastic scintillator yields better results (100). Both detectors are matched for equal count rates in the Compton region by adapting the source–detector geometry and the pulse heights are equalized by means of the gain of the respective linear amplifiers. To correct for the unequal absorption of the gamma rays in both detector, a lead grid has to be placed in front of the plastic detector, in order to obtain correct compensation. The detectors are operated simultaneously, the NaI(Tl) in the positive storage mode and the compensation detector in the negative mode, by means of a multichannel analyzer equipped with a mixing panel. As can be seen from Figure 6.39 a spectrum with net photopeaks is obtained. A schematic drawing of the apparatus is also shown in the same figure. With this spectrometer, adequate compensation is obtained for gammaenergies between 0.15 and 2.7 MeV. It has to be noticed however that compensation becomes difficult when dealing with mixtures of isotopes showing large differences in countrates.

(F) Absolute Counting Techniques

In some cases of neutron activation analysis, the knowledge of the disintegration rate of a source can be required. This can happen when determining neutron fluxes as described in chapter 3, section VI, B.

Depending on the decay scheme and on the physical state of the isotope, one can apply the following techniques:

A calibrated G.M. counter or a calibrated gama spectrometer;
A 4π gas-filled counter;
A liquid scintillation counter;
Absolute gamma spectrometry;
Gamma-gamma or beta-gamma coincidence

In the first case, a sample is measured in the same geometry as a calibrated source. When use is made of a G.M. counter any source of known disintegration rate can be used as a standard, provided sample and standard are corrected for self absorption and external absorption, as is described in section III, C, 1 of this chapter. It is however recommended to have a standard with an E_{max} of the beta spectrum, which is in the vicinity of the E_{max} of the sample.

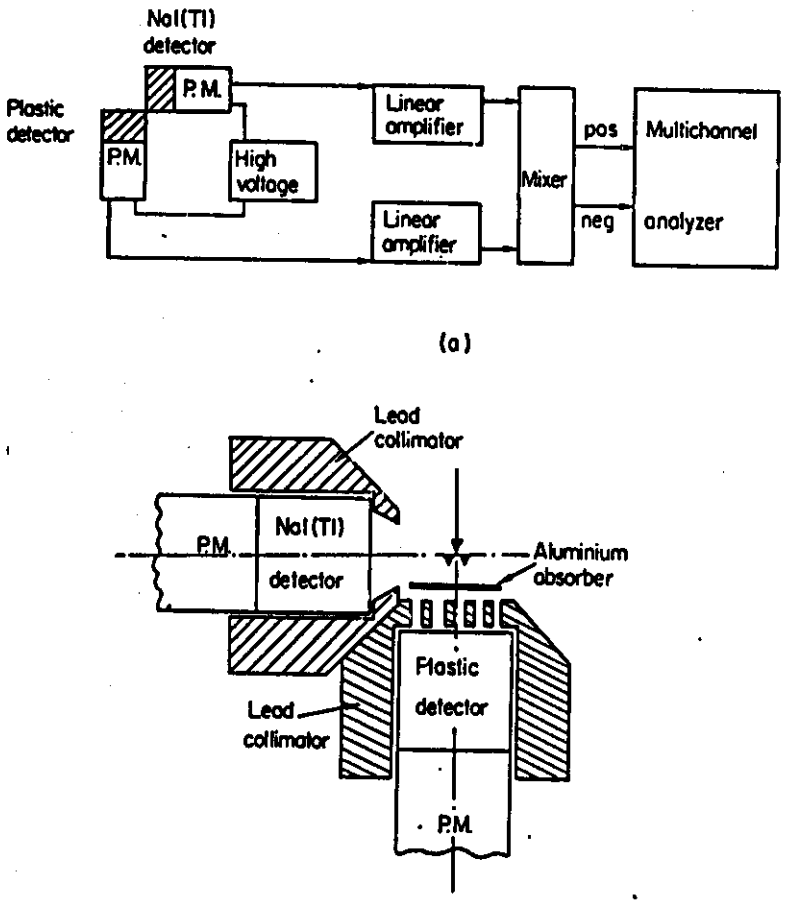

Fig. 6.39. Principle diagram and geometrical arrangement of a Compton subtraction spectrometer (a) and complex gamma spectrum of a mixture of radionuclides.

As the intrinsic efficiency of a gamma detector is a function of the energy, a gamma spectrometer has to be calibrated with a standard emitting the same gamma energy as the sample. When no such standard is available, one can use two calibrated standards having respective energies closely above and below the energy of the samples. Subsequently an interpolation can be performed, which can be either linear or can make use of the efficiency curves for the gamma detector (see

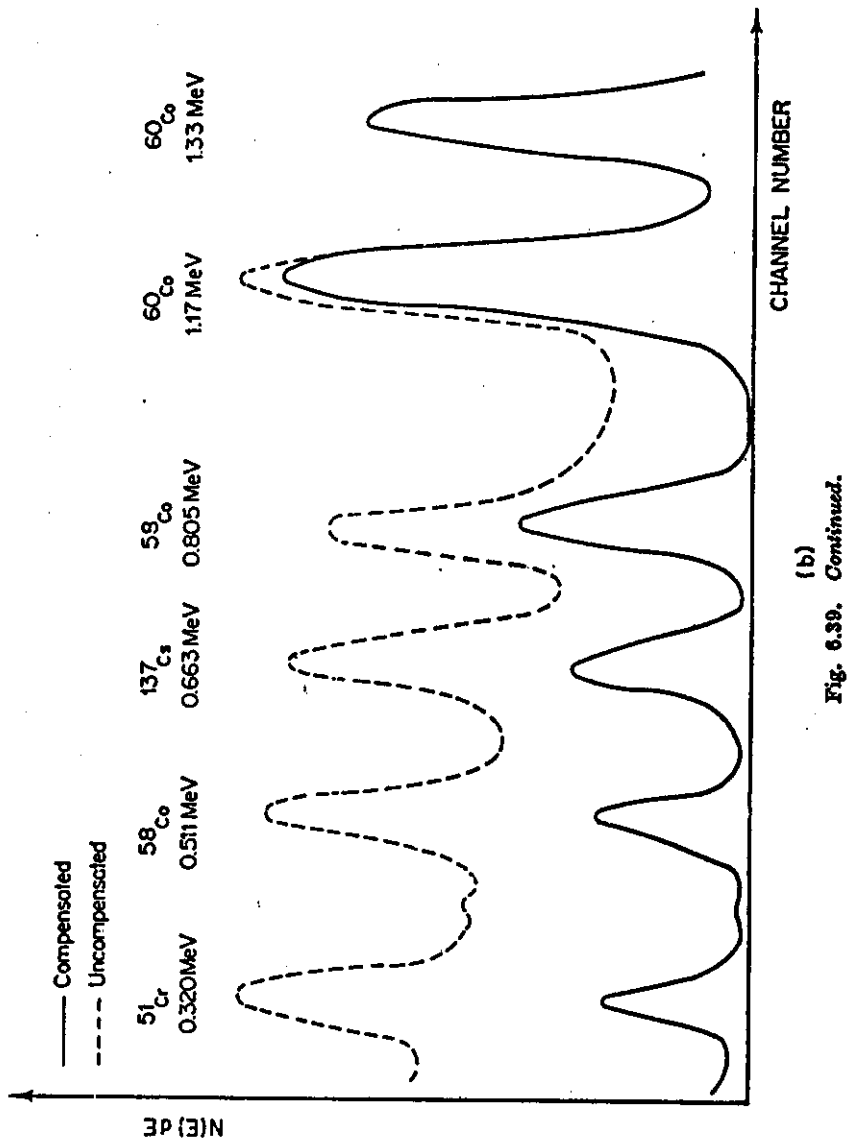

(b)

Fig. 6.39. *Continued.*

^{32}P measurement in the presence of ^{35}S at two sufficiently high amplifier gain settings is given in Figure 6.40. From Figure 6.40 it also appears that discrimination between beta emitters of different energies is possible.

When dealing with a pure gamma emitter, the sample can be calibrated using absolute gamma spectrometry. In this technique, described by Heath (69), the absolute efficiency z of the detector is used to calculate the disintegration rate D of the sample by means of the activity measured under a photopeak A_p as follows:

$$D = \frac{A_p}{zPqA} \tag{6.63}$$

P is the ratio of the activity under the photopeak to the total activity in the spectrum, described as the peak-to-total ratio. q is the branching factor for the measured gamma ray, which is the percent occurrence of the transition in the decay scheme. A represents a correction factor for absorption in the sample and in the can of the detector. Due to the large penetrating power of gamma rays, A will in most cases equal 1. The values for z and P as a function of the gamma ray energy and the source detector distance are given in the literature (see section III, D of this chapter) whereas q can be obtained from the decay scheme (see section I, B of this chapter).

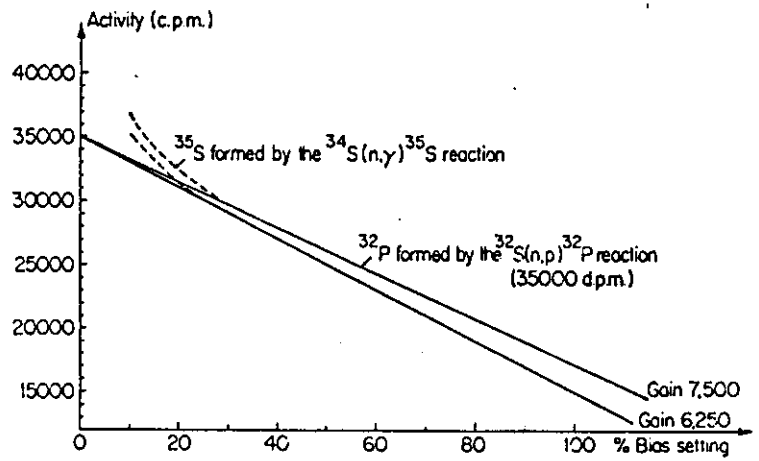

Fig. 6.40. Absolute measurement of the ^{32}P activity (E_{max} = 1.7 MeV) in the presence of ^{35}S (E_{max} = 0.167 MeV), by liquid scintillation counting. The isotopes are produced by irradiation of $(NH_4)_2SO_4$ in a nuclear reactor.

When beta–gamma or gamma–gamma cascades occur in the decay scheme of an isotope, the absolute disintegration rate D can be found by measuring both components of the cascade by means of a coincidence technique, described in section III, E, 1 of the same chapter. Indeed, combining equations (6.49) and (6.51) one obtains:

$$D = \frac{R_1 R_2}{R_c} \tag{6.64}$$

From equation (6.64) it appears that D can be calculated from the count rates in both detectors R_1 and R_2 and from the coincidence count rate R_c. Although this technique requires a rather complicated equipment, it is very easy to perform, and yields excellent results.

A study of the decay scheme of the isotope to be measured is necessary, for instance to take into account the branching and conversion factors of the measured transition.

References

1. De Boeck, R., Adams, F., and Hoste, J., *J. Radioanalyt. Chem.*, 1, 397 (1968).
2. Gamow, G., and Critchfield, C. L., *Theory of the Atomic Nucleus and Nuclear Energy Sources*, Clarendon Press, Oxford (1949).
3. Haissinsky, M., *Nuclear Chemistry and its Applications*, Addison-Wesley Publ. Co., London (1964).
4. Evans, R. D., *The Atomic Nucleus*, McGraw-Hill Book Co., London (1955).
5. Lindner, R., *Kern und Radiochemie*, Springer-Verlag, Berlin (1961).
6. Reitz, J. R., *Phys. Rev.*, 77, 10 (1950).
7. *Nuclear Data Sheets*; N.C.R., Washington D.C. (U.S.A.).
8. Lederer, C. M., Hollander, J. M., and Perlman, I., *Table of Isotopes, 6th edition*, J. Wiley and Sons, London (1967).
9. Kunz, W., and Schintlmeister, J., *Nuclear Tables*, Pergamon Press, London (1963).
10. Dzhelepov, B. S., and Peker, L. K., *Decay Schemes of Radioactive Nuclei*, Pergamon Press, London (1961).
11. Boyadjov, I., De Neve, R., and Hoste, J., *Anal. Chim. Acta*, 40, 373 (1968).
12. Fermi, E., *Z. Physik*, 88, 161 (1934).
13. Gamow, G., and Teller, E., *Phys. Rev.*, 49, 895 (1936).
14. Sargent, B. W., *Proc. Roy. Soc.* (London), A 139, 659 (1933).
15. Mayer, M. G., Moszkowski, S. A., and Nordheim, L. W., *Rev. Mod. Phys.*, 23, 315 (1951).
16. Konopinski, E. J., *Rev. Mod. Phys.*, 15, 209 (1943).

17. Bohr, N. *Phil. Mag.*, 30, 581 (1915).
18. Gleason, G. J., Taylor, J. D., and Tabern, D. L., *Nucleonics*, 8(5), 12 (1951).
19. Schulze, W., *Neutronenaktivierung als Analytisches Hilfsmittel, Die Chemische Analyse*, Band 50, F. Enke Verlag, Stuttgart (1962).
20. Llewellyn-Jones, F., *Ionization and Breakdown in Gases*. Science paperbacks – Chapman and Hall Ltd., London (1966).
21. Fassbender, H., *Einführung in die Messtechnik der Kernstrahlung und die Anwendung der Radioisotope*, Georg Thieme Verlag, Stuttgart (1962).
22. Lox, F., and Eeckhaut, Z., *Rev. Sci. Instr.*, 40, 1206 (1969).
23. Parekh, C. H., *J. Sc. and Ind. Res.*, 20 D, 13 (1961).
24. Curran, S. C., *Luminescence and the Scintillation Counter*, Butterworths, London (1953).
25. Morton, G. A., *1st Geneva Conference U.N.*, Proceedings 14, 246, New York (1962).
26. Riehl, N., *Ann. Phys.*, 29, 636 (1937).
27. Wannier, G., *Phys. Rev.*, 52, 191 (1937).
28. Dearnaley, G., and Northrop, D. C., *Semiconductor Counters for Nuclear Radiations*, Spon Ltd., London (1966).
29. Taylor, J. M., *Semiconductor Particle Detectors*, Butterworths, London (1963).
30. Gibbons, D. E., and Northrop, D. C., *Proc. Phys. Soc.*, 80, 276 (1962).
31. Mott, N. F., *Proc. Roy. Soc.*, A 171, 27 (1939).
32. Schottky, W., *Z. Phys.*, 113, 367 (1939).
33. Pell, E. M., *J. Appl. Phys.*, 31, 291 (1960).
34. Adams, F., *Atomic Energy Rev.* (I.A.E.A.), 5(4), 31 (1967).
35. Dearnaley, G., *Journ. Brit. I.R.E.*, 24, 153 (1962).
36. Adams, F., and Dams, R., *Radiochim. Acta*, 10, 1 (1968); *J. Radioanalyt. Chem.*, 3, 99 (1969).
37. De Boeck, R., Adams, F., and Hoste, J., *Anal. Chim. Acta*, 39, 270 (1967).
38. Parekh, C. H., *Nucl. Instr. and Meth.*, 15, 213 (1962).
39. Vassos, B. H., Berlandi, F. J., Neal, T. E., and Mark Jr., H. B., *Anal. Chem.*, 37, 1653 (1965).
40. Rosanovitch, A., *J.A.R.I.*, 3, 251 (1958).
41. Aten Jr., A. H. W., *Nucleonics*, 6(1), 68 (1950).
42. Davidson, J. D., and Feigelson, P., *J.A.R.I.*, 2, 1 (1957).
43. Rapkin, E., *J.A.R.I.*, 15, 69 (1964).
44. Faissner, H., Ferrero, F., Ghani, A., and Reinharz, M., *Nucleonics*, 21(2), 50 (1963).
45. Steinberg, D., *Nature*, 182, 740 (1958).
46. Steinberg, D., *Nature*, 183, 1253 (1959).
47. Steinberg, D., *Anal. Biochem.*, 1, 23 (1960).
48. Funt, B. L., *Nucleonics*, 14(8), 83 (1956).
49. White, C. G., and Helf, S., *Nucleonics*, 14(10), 46 (1956).
50. Pauwels, M., Gijbels, R., and Hoste, J., private communication.
51. De Soete, D., De Neve, R., and Hoste, J., *Mod. Trends in Activation Analysis*, Proceedings, Texas (1965), p. 31.
52. Flammersfeld, A., *Z. Naturforsch.*, 2a, 370 (1947).

53. Glendenin, L. E., *Nucleonics*, 2 (1), 12 (1948).
54. Glendinin, L. E., and Coryell, C. D., U.S.A.E.C. Report MDDC-19 (1946).
55. Feather, N., *Proc. Camb. Phil. Soc.*, 34, 599 (1938).
56. Gijbels, R., and Hoste, J., *Anal. Chim. Acta*, 29, 289 (1963).
57. De Waard, H., *Nucleonics*, 13, 36 (1955).
58. Fite, L. E., Gibbons, D., and Wainerdi, R. E., *Mod. Trends in Activation Analysis*, Proceedings, Texas (1961), p. 102.
59. Dudley, R. A., I.A.E.A. *Symp. on Radiochem. Meth. of Anal.*, Proceedings II, 69, Salzburg (1964).
60. Chase, R. L., *Tran. Nucl. Sci.*, I.R.E., NS-9(1), 119 (1962).
61. Scherbatskoy, S. A., *Rev. Sci. Instr.*, 32, 599 (1961).
62. Covell, D. F., *Nucl. Instr. and Meth.*, 47, 125 (1967).
63. Hickok, R. L., and Draper, J. E., *Rev. Sci. Instr.*, 29, 994 (1958).
64. Kelley, G. G., Bell, P. R., Davis, R. C., and Lazar, N. H., *Nucleonics*, 14(4), 53 (1956).
65. De Soete, D., and Hoste, J., *Nucleonics*, 20(4), 72 (1962).
66. Fano, V., *Phys. Rev.*, 72, 26 (1947).
67. Mann, H. M., *Bull. Am. Phys. Soc.*, 11, 127 (1966).
67a. Bilger, H. R., *Phys. Rev.*, 163, 238 (1967).
68. Crouthamel, C. E., *Applied Gamma Ray Spectrometry*, Pergamon Press, London (1960); 2nd ed., revised and enlarged by Adams, F., and Dams, R. (1970).
69. Heath, R. L., *Scintillation Spectrometry*, Phillips Petr. Co., I and II IDO-16880-1, IDO-16880-2 (1964).
70. Grosjean, C. C., and Bossaert, W., *Table of Absolute Detection Efficiencies, Computing Laboratory of University of Ghent*, Belgium (1965).
71. Cline, J. E., and Heath, R. L., *Gamma-Ray Spectrometry of Neutron-Deficient Isotopes, Ann. Progress Rept.*, Phillips Petr. Co., IDO-17222 (1967).
72. Heath, R. L., and Cline, J. E., *Gamma-Ray Spectrometry of Neutron-Deficient Isotopes; Ann. Progress Rept.*, Phillips Petr. Co., IDO-17188 (1966).
73. Cuypers, M., and Cuypers, J., *Gamma-Ray Spectra and Sensitivities for 14 MeV Neutron Activation Analysis*, Texas A. & M. University (1966).
74. Strain, J. E., and Ross, W. J., *14 MeV Neutron Reactions*, ORNL-3672, (1965).
75. Connally, R. E., and Leboeuf, M. B., *Anal. Chem.*, 25, 1095 (1953).
76. McIsaac, L. D., *U.S. Naval Radiol. Def. Lab., Rept.*, USNRDL-TR-72 (1956).
77. Covell, D. F., *Anal. Chem.*, 31, 1785 (1959).
78. Helmer, R. G., Heath, R. L., Schmittroth, L. A., Jayne, G. A., and Wagner, L. M., *Nucl. Instr. and Meth.*, 47, 305 (1967).
79. Schonfeld, E., *Nucl. Instr. and Meth.*, 52, 177 (1967).
80. Heath, R. L., Helmer, R. G., Schmittroth, L. A., and Cazier, G. A., *Nucl. Instr. and Meth.*, 47, 281 (1967).
81. Yule, H. P., *Anal. Chem.*, 38, 103 (1966).
82. Salmon, L., *Nucl. Instr. and Meth.*, 14, 193 (1961).

83. Johnson, ... E., *Tran. Am. Nucl. Soc.*, 10, No. 1, 86 (1967).
84. Kim, J. I., Speecke, A., and Hoste, J., *Anal. Chim. Acta*, 33, 123 (1965).
85. Hoogenboom, A., *Nucl. Instr.*, 3, 57 (1958).
86. Wahlgren, M., Wing, J., and Hines, J., *Mod. Trends in Activation Analysis*, Proceedings, Texas (1965), p. 154.
87. Schulze, W., *Modern Trends in Activation Analysis*, Proceedings, Texas (1965), p. 272.
88. Albert, R. D., *Rev. Sci. Instr.*, 24, 1096 (1953).
89. Cooper, R. D., Lineken, D. M., and Brownell, G. L., I.A.E.A. *Symposium on Nuclear Activation Techniques in the Life Science*, SM-91/60, Amsterdam (1967).
90. Bell, P. R., *Science*, 120, 625 (1953).
91. Perkins, R. S., I.A.E.A. *Symposium on Radiochem. Meth of Anal.*, Proceedings II, 47, Salzburg (1964).
92. Palms, J. M., Wood, R. E., and Puckett, O. H., *IEEE Tran. Nucl. Sci.*, NS-15 (3), 397 (1968).
93. Sayres, A. R., and Baicker, J. A., Paper presented at the 11th scintillation and semiconductor counter Symposium, Washington D.C., Feb. 28 (1968).
94. Kraner, H., and Chase, R. L., Paper presented at the 11th scintillation and semiconductor counter Symposium, Washington D.C., Feb. 28 (1968).
95. Tamm, U., Michaelis, W., and Coussieu, P., *Nucl. Instr. and Meth.*, 48, 301 (1967).
96. Strauss, M. G., and Larsen, R. N., *Nucl. Instr. and Meth.*, 56, 80 (1967).
97. Alexander, T. K., Pearson, J. D., Litherland, A. E., and Broude, C., *Phys. Rev. Letters*, 13, 86 (1964).
98. Peirson, D. H., *Nature*, 173, 990 (1954).
99. Peirson, D. H., *Brit. Journ. Appl. Phys.*, 6, 444 (1955).
100. De Soete, D., and Hoste, J., *Radiochim. Acta.*, 4, 35 (1965).
101. Pate, B. D., and Yaffe, L., *Can. Journ. of Chem.*, 33, 15 (1955).
102. Pate, B. D., and Yaffe, L., *Can. Journ. of Chem.*, 33, 610 (1955).
103. Pate, B. D., and Yaffe, L., *Can. Journ. of Chem.*, 33, 929 (1955).
104. Pate, B. D., and Yaffe, L., *Can. Journ. of Chem.*, 33, 1656 (1955).
105. Pate, B. D., and Yaffe, L., *Can. Journ. of Chem.*, 34, 265 (1956).
106. Glendenin, L. E., and Flynn, K. F., *Phys. Rev.*, 116(3) (1959).
107. Vaninbrouckx, R., and Spernol, A., *J.A.R.I.*, 16, 289 (1965).
108. White-Grodstein, G., N.B.S. Circular 583 (1957).
109. Hubbel, J. H., and Berger, M. J., N.B.S. Report 8681 (1966).

CHAPTER 7

PREPARATION OF SAMPLES AND STANDARDS

The preparation of samples and standards is of great practical importance. If possible, the analyst himself should carry out all processing of material under controlled conditions, or at least be aware of the detailed history of the sample, so that he can take any necessary steps to remove surface contamination before or after activation is carried out.

Commensurate with availability, sensitivity requirements, dimensions of the container, matrix activity and macroscopic cross section, sample weights are usually maximized.

If the impurity content of the sample is approximately known, the sample size can be estimated for a given irradiation condition (flux, irradiation time, . . .).

In most cases the problem of the standard is not so difficult as in other physical methods of analysis, such as emission spectrography, X-ray fluorescence, etc., since matrix or third-element effects are less important. However, neutron shielding is possible (see Chapter 10), and should be eliminated or at least kept equal for standards and samples. Absorption of emitted radiation in the sample must also be taken into account.

The irradiation time for a given flux is mostly chosen considering the saturation factor for the radionuclide of interest, $[1 - \exp(-\lambda t_b)]$.

For 14 MeV neutron activation, the irradiation time is kept as short as possible to prevent untimely exhaustion of the tritium target.

I. Preparation of Samples

(A) Sampling of Solid Samples

Massive solids can be wrapped in aluminium foil and packed in standard aluminium cans for irradiation.

Solid samples may be too large for direct irradiation so that it may be necessary to reduce the sample size by grinding, cutting, drilling, etc. before packing. Hard steel tools, used for this purpose or for cleaning